#2
DUP

INVESTIGATION OF RHEOLOGICAL PROPERTIES OF AERIAL-DELIVERED FIRE RETARDANT

EXTENDED STUDY

Final Report

to

DUGWAY PROVING GROUND
TECHNICAL LIBRARY

UNITED STATES DEPARTMENT OF AGRICULTURE
FOREST SERVICE
INTERMOUNTAIN FOREST & RANGE EXPERIMENT STATION

A report of research performed under the auspices of the Intermountain Forest and Range Experiment Station, Ogden, Utah.

5333 224
CB-148752
5333 224

Shock Hydrodynamics
A DIVISION OF Whittaker

INVESTIGATION OF RHEOLOGICAL PROPERTIES OF AERIAL-DELIVERED FIRE RETARDANT EXTENDED STUDY

FINAL REPORT
(8990-05)

by

W.H. Andersen
R.E. Brown
N.A. Louie
P.J. Blatz
J.A. Burchfield

Contract 26-3198

Period Covered 17 June 1974 Through 16 December 1974

16 December 1974

Intermountain Forest & Range Experiment Station

USDA Forest Service

Ogden, Utah 84401

The research conducted under this contract is a part of a program to improve fire control technology, specifically through the use of fire retardant chemicals and delivery systems whose chemical and/or design characteristics are tailored to fuel and fire situation needs. This program is being conducted at the Northern Forest Fire Laboratory. Information or questions regarding these studies should be directed to the:

Northern Forest Fire Laboratory
Drawer G
Missoula, Montana 59801

SHOCK HYDRODYNAMICS DIVISION, WHITTAKER CORPORATION
4710-16 Vineland Avenue, North Hollywood, California 91602

ACKNOWLEDGEMENT

The authors wish to acknowledge the helpful comments of Mr. Charles W. George, Contract Monitor, U. S. Forest Service.

TABLE OF CONTENTS

		Page
	SUMMARY	viii
1.	INTRODUCTION	1
2.	MEASUREMENT OF FLUID ELASTICITY AND YIELD STRESS	1
	2.1 Viscous and Elastic Nature of Fire Retardant Solutions	1
	2.2 Elasticity Measurements	2
	2.2.1 Experimental Results	5
	2.2.2 Effective Viscosity	11
	2.3 Yield Stress Measurements	13
	2.3.1 Experimental Results (Inclusion of Low Shear Rate Data)	14
	2.3.2 Observations of Stress Relaxation	14
3.	EXTENDED LIQUID BREAKUP ANALYSIS AND CORRELATION	16
	3.1 Terminal Droplet Size Produced by Initial Peripheral Wind Stripping	16
	3.1.1 Number Distribution of Droplets	16
	3.1.2 Mass Distribution of Droplets	18
	3.1.3 Relative Rates of Liquid Stripping	20
	3.2 Terminal Droplet Size Produced in the Effective Ground Pattern	22
	3.2.1 Liquid Velocity Reduction by Air Drag	22
	3.2.2 Evaluation of Velocity Reduction	23
	3.2.3 Average Terminal Droplet Size	25
	3.2.4 Droplet Size Distribution	27
	3.2.5 Additional Considerations	27
	3.3 Droplet Settling	33
	3.3.1 Wind Drift	34
	3.4 Ground Contour Pattern	36
	3.4.1 Ground Path Length	36
	3.4.2 Ground Path Width and Area	40

TABLE OF CONTENTS (Cont'd)

Page

4. RETARDANT IMPACTION AND FLOW ON FUELS 42

4.1 Experimental Studies 42

4.1.1 Results of the Drop Spreading Experiments 43
4.1.1.1 Effect of Impact Velocity and Drop Size 46
4.1.2 Drop Impact with a Wood Dowel Length 46

4.2 Analytical Studies 46

4.2.1 Static Spread of a Liquid Drop 46
4.2.2 Model of Dynamic Drop Spread Using an Assumed Flow Field 52
4.2.3 Model of Dynamic Drop Spread Based on Energy Conservation 53

5. CONCLUSIONS 57

5.1 Retardant Properties During Aerial Dissemination 58

5.2 Recommendations 59

REFERENCES 61

APPENDIX I - VELOCITY AND DISPLACEMENT OF FALLING DROPS 62

APPENDIX II - LIQUID SPREADING CONTROLLED BY SURFACE TENSION . 64

APPENDIX III - APPROXIMATE MODEL FOR DROP SPREAD BASED ON ENERGY CONSERVATION CONCEPTS 65

LIST OF FIGURES

FIGURE	TITLE	PAGE
1a	Measuring Head of the Rotovisco	3
1b	Rotovisco with ELZ Visco-Elastic Attachment	3
2	Measured Elastic Deformation Angle of Phos-Chek vs Shear Rate at 20°C	6
3	Measured Elastic Deformation Angle of Fire-Trol 931 vs Shear Rate at 20°C	7
4	Recoverable Shear vs Shear Rate for Phos-Chek XA at 20°C	9
5	Estimated Recoverable Shear vs Shear Rate for Fire-Trol 931 at 20°C	10
6	Effective Viscosity of the Fire Retardant Solutions as a Function of Shear Rate	12
7	Methods Employed for the Estimation of Yield Stress	15
8	Computed Number Size Distribution of the Droplets Produced by the Initial Peripheral Stripping of the Liquid Fire Retardants	17
9	Computed Mass Size Distribution of the Droplets Produced by the Initial Peripheral Stripping of the Liquid Fire Retardants	19
10	Comparison of the Initial Droplet Size Distribution Computed Using the Log Normal and Mayer Distribution Functions	21
11	Computed Final Average Droplet Sizes in the Effective Ground Pattern	26
12	Computed Final Size Distribution of the Droplets in the Effective Ground Pattern	28
13	Photographic Sequence of the Aerodynamic Breakup Behavior of a Drop of Phos-Chek at a Wind Velocity of 90 ft/sec	31
14	Selected Frames from Photographic Sequences of the Impaction of Drops of Various Liquid Retardants with Cardboard	44

LIST OF FIGURES (Concluded)

FIGURE		PAGE
15	Comparison of the Spreading Behavior of Drops of the Retardants Impacting with a Cardboard Surface	45
16	Effect of Impact Velocity and Drop Size on the Spreading Behavior of Fire-Trol 100	47
17	Selected Frames From the Impact of a Falling Drop of Phos-Chek with a 1/8" Diameter Wood Dowel	48
18	Selected Frames From the Impact of a Falling Drop of Fire-Trol 100 with a 1/4" Diameter Wood Dowel	50
19	Comparison of Theoretical Liquid Spreading Rate with Experiment.	54
20	Theoretical Drop Spreading Curves for the Fire Retardants . .	55
21	Theoretical Curves Showing Parameter Effects on Liquid Drop Spreading	56
22	Summary of the Shear Rate and Viscosity of the Various Liquid Fire Retardants During Aerial Dissemination	60

LIST OF TABLES

TABLE	TITLE	PAGE
I	Instrument Constants for the RVI Haake Rotoviscometer with ELZ Viscoelastic Attachment	5
II	Computed Effect of System Parameters on the Velocity Reduction of Liquid Retardants While Undergoing Breakup by Taylor Instability	24
III	Computed Final Average Droplet Sizes in the Effective Ground Pattern.	25
IV	Estimated Terminal Droplet Velocity	33
V	Estimated Wind Drift of the Settling Droplets	34

LIST OF TABLES (Concluded)

TABLE	TITLE	PAGE
VI	Estimated Properties of the Droplets Assuming a One-Third Power Viscosity Dependence on Droplet Size	36
VII	Estimated Horizontal Path Length of Traveling Falling Droplets	39

Use of trade or firm names is for reader information only, and does not constitute endorsement by the U. S. Department of Agriculture of any commercial product or service.

SUMMARY

This report describes the results of additional studies that were conducted on an earlier program,[1] whose purpose was to establish the relationships between the rheological properties of a liquid fire retardant and the aerial drop behavior, dispersion characteristics, and wetting-out properties of the retardant.

Experimental studies were conducted to measure the fluid elasticity of the retardants Phos-Chek XA, Fire-Trol 100 and Fire-Trol 931, using a Haake Rotoviscometer with ELZ Viscoelastic attachment. These studies corroborated the previous hypothesis that Fire-Trol 100 - which is a clay thickened retardant - is nonelastic in flow. However Fire-Trol 931 was found to be elastic in nature, although not to the degree that Phos-Chek is - especially at the higher shear rates. The elasticity may be due to the polyphosphate groups. The measured elasticity of gum-thickened Phos-Chek at low shear rates was found to be significantly greater than that determined previously by the capillary tube technique. However the extrapolated measurements are in good agreement with those determined previously at high shear rates. Additional measurements were also made of the yield stress of the retardants, and the results are essentially in agreement with those determined previously.

Further analytical studies were conducted toward understanding the aerodynamic breakup, dispersion and settling properties of the retardants. It is shown that liquid deceleration accompanies the Taylor breakup of the liquid, and that the terminal droplet size of the retardant is consequently larger (by about a factor of two) in the effective ground pattern region than in the initial peripheral wind stripping region. The terminal droplet size distributions in both regions are estimated for the three preceding retardants and water - using the new effective viscosity data - and the effects of the various factors and parameters discussed. On the basis of the new effective viscosity data the terminal droplet size of the two Fire-Trol retardants are estimated to be about the same, but are significantly smaller than that of Phos-Chek. Water droplets are much smaller still.

The effects of size on the dispersion and settling of the droplets is discussed. Small droplets undergo longer settling times and wind drift than larger droplets, and estimates are given for the various retardants. Large particles undergo projection effects which can result in increased path length. The various factors and sequence of events leading to ground coverage and contour pattern are also discussed further.

Experimental measurements using high speed photographic techniques were made of the impaction and spreading of individual drops of retardant falling on a rigid cardboard surface. The rate of spreading decreases with increase in viscosity of the retardant, and the final spread factor (reciprocal film thickness) also decreases in this order. Increase in drop size and decrease in impact velocity cause a decrease in the spread factor. An approximate analytical model is developed which describes the liquid spreading in terms of the important impact and fluid parameters, including drop size, impact velocity and fluid viscosity. The experimental measurements are correlated with the theory.

Photographs were also obtained of the impaction of retardant drops with a wood length dowel (simulating a branch or twig). The impaction causes a sheet of liquid to flow laterally away on both sides from the dowel. For Fire-Trol 100 the sheet width remains essentially constant until the liquid source is depleted, at which time it fractures lengthwise near the dowel. For Phos-Chek however, the width of the sheet gradually decreases, and finally necks down to a ligament before fracture. This behavior is probably related to the elasticity of the flowing liquid. There is no evidence for liquid wrap-around of the dowel for either liquid.

A brief discussion is presented of the implications and uncertainties of the studies, and a summary presented of the shear rate and effective viscosity of the liquid retardants during the various stages of dissemination. Recommendations are made for additional studies that could lead to a further improved understanding of the aerial dissemination of liquid retardants.

1. INTRODUCTION

Aircraft have been used for many years to deliver liquid fire retardant solutions to large fires, and over the years a variety of fire retardants, aircraft, and tank and gating systems have been used in fighting fires. During this time it became apparent that the rheological properties of the liquid retardant can have a significant effect on the aerodynamic breakup and dispersion characteristics of the retardant subsequent to its release from the aircraft - which will affect both the particle size of the retardant that interacts with the fuel complex on the ground, and the localized area concentration of the dispersed retardant. It was also found that the rheological properties of the retardant solution can influence the wetting-out characteristics of a fuel element (e.g., brush or tree) by the retardant rain.

Recognizing the need for an improved understanding of the effects of the fluid rheological properties in using aerial delivered fire retardant solutions, the U. S. Forest Service sponsored a program with Shock Hydrodynamics, whose overall purpose was to establish the relationships between the rheological properties of a liquid fire retardant and the drop behavior, breakup and dispersion characteristics, and wetting-out properties of the retardant. This program was completed in June 1974, and is described in ref. 1. On the basis of the results obtained on this initial program and the more recent availability of certain new attachments for the Rotoviscometer, the program was extended in order to better fulfill its objectives. This report describes the results of these additional studies.

In the sections to follow there is first presented the results of the additional measurements of the rheological properties of the current liquid fire retardant solutions of interest using the new Rotoviscometer attachments. This is followed by further analysis and discussion of the aerodynamic breakup, dispersion and settling properties of the retardants, and of the factors that control the ground concentration pattern. The results of the extended studies on the flow behavior of the retardants during dynamic impaction with a fuel are then described. The report concludes with a brief discussion of additional studies that could usefully be conducted to advance the state of the art in the development of aerial-delivered liquid fire retardants.

2. MEASUREMENT OF FLUID ELASTICITY AND YIELD STRESS

2.1 VISCOUS AND ELASTIC NATURE OF FIRE RETARDANT SOLUTIONS

A thickener is added to a fire retardant solution in order to increase its viscosity and consequently its terminal droplet size. However in ref. 1 it was shown that it is the effective viscosity, η_e, that controls the aerodynamic breakup behavior and final droplet size of an aerially delivered fire retardant, and that the effective viscosity is related to the apparent viscosity, η, and recoverable shear (elastic strain), s, of the fluid by the equation

$$\eta_e = \eta (1 + s) \tag{1}$$

where the value of both η and s may depend on the shear rate of the liquid while it is undergoing breakup. Terminal droplet size increases with increase in η_e. For a nonelastic liquid, s is zero; while for a Newtonian liquid, η is

constant and is independent of shear rate.

On the previous program measurements were made of the viscous properties of the contemporary liquid retardants Phos-Chek XA, Fire-Trol 100 and Fire-Trol 931, using both the high pressure capillary tube and rotoviscometer techniques. It was found that all of these retardants are non-Newtonian in nature and undergo shear thinning, which causes the apparent viscosity exhibited during breakup to be much less than that measured by the normal (low shear rate) Brookfield viscometer. Measurements were also made of the elastic behavior (expressed as recoverable shear) of Phos-Chek as a function of shear rate, using the capillary tube technique. It was found that the recoverable shear increases with increase in shear rate, which causes the effective viscosity of Phos-Chek to remain relatively high during breakup. This results in a relatively large final droplet size of the aerially dispersed liquid. The significant elastic behavior of Phos-Chek while undergoing shear is attributed to the fact that Phos-Chek is a gum thickened retardant. The elastic behavior of Fire-Trol 100 and Fire-Trol 931 was not measured on the previous program - due to lack of time - but it was surmised that these retardants are essentially non-elastic in nature since Fire-Trol 100 is a clay thickened retardant, while Fire-Trol 931 is a relatively short chained polyphosphate substance.

Since that time certain new attachments have become available for the rotoviscometer which allow the measurement of fluid elasticity (and yield stress) by this instrument. These attachments have enabled the measurement of the elastic properties of Fire-Trol 100 and 931, as well as those of Phos-Chek for comparison with the results obtained using the capillary tube technique. New measurements of the yield stress of the retardant solutions were also made for comparison with those obtained previously.

2.2 ELASTICITY MEASUREMENTS

The measurements were made using the Model RV1 Haake Rotoviscometer with ELZ Visco-Elastic attachment, which was obtained on loan from the Forest Service. A schematic of the measuring head of the Rotovisco is shown in Figure 1a. The power to drive the rotor is transmitted to the measuring head through a 10-position geared transmission and a flexible drive cable. There is interposed between the drive cable and the rotor a precision torsion spring. The viscous drag on the rotor at any constant shear rate causes a deflection or twisting of the torsion spring, and this action is sensed by a brush potentiometer within the measuring head. The signal generated by the potentiometer is thus directly related to the torque on the rotor caused by the viscous drag. This signal is transmitted by electrical leads within the same flexible shaft which houses the flexible drive cable. The signal output is read on the instrument dial on the control panel, or on an external recorder.

The ELZ Visco-Elastic attachment allows the measurement of the restoring moment of the rotor under the effect of the fluid elasticity (Figure 1b). A coupling shaft is attached between the measuring head and the rotor. This coupling device permits the rotor to be manually connected to - or disconnected

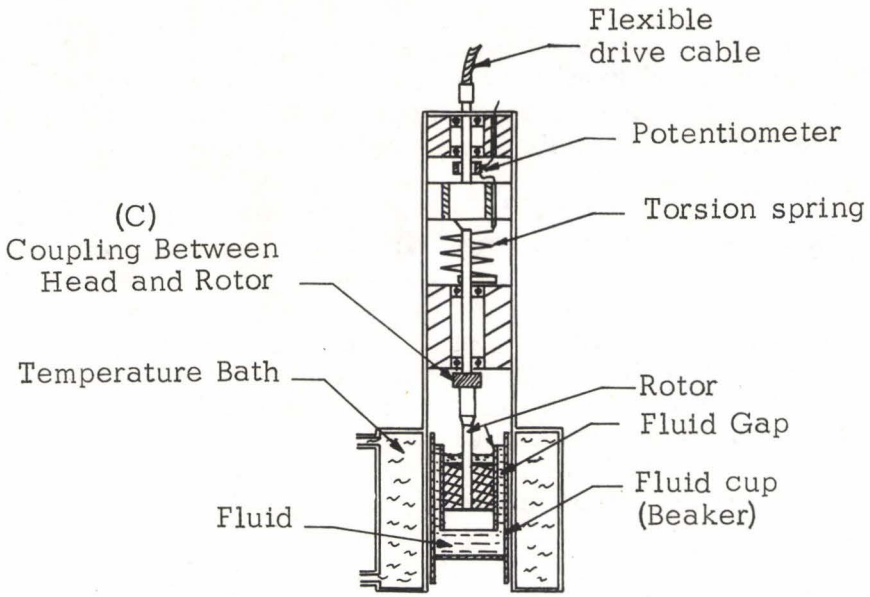

Figure 1a. Measuring Head of the Rotovisco.

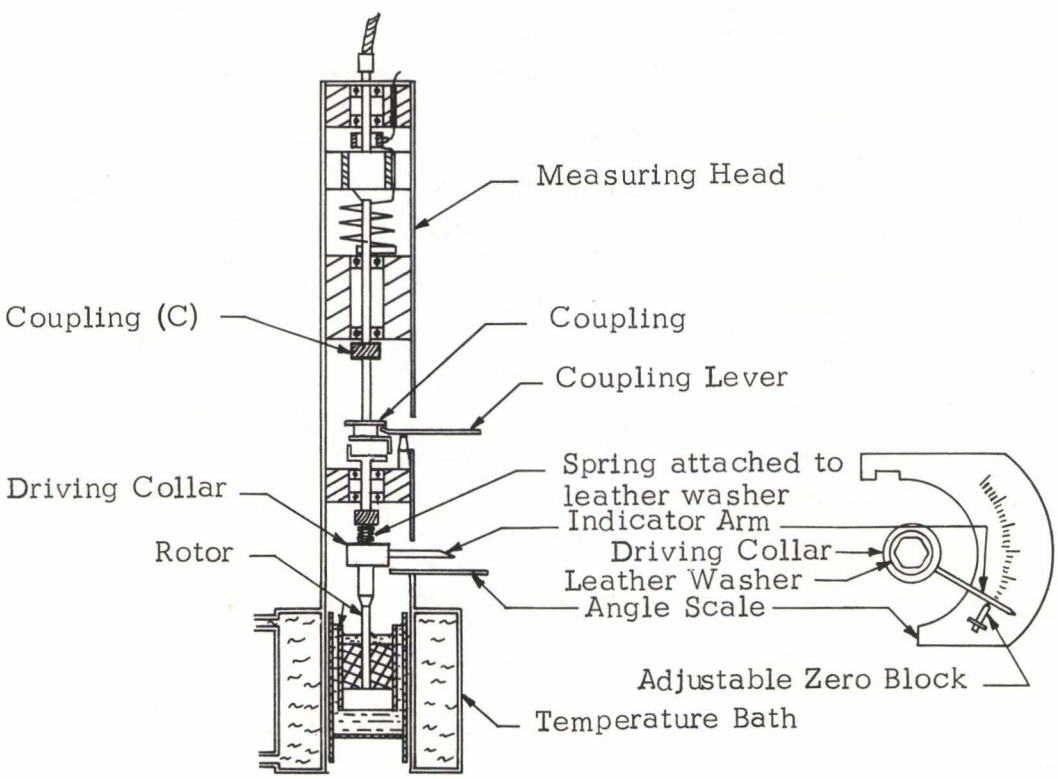

Figure 1b. Rotovisco with ELZ Visco-Elastic Attachment.

from - the measuring head. A disconnection is accomplished by pushing the coupling lever down. If the fluid exhibits elastic behavior, the sudden termination of rotational torque causes the rotor to spring back, or relax. The angular displacement of this restoration is directly related to the elastic strain.

A "driving collar" with an indicating arm is mounted on the rotor shaft for the elasticity measurements. The driving collar serves the following purposes:

(a) The indicator arm which records the angular relocation after the rotor rotation is interrupted is connected onto a ring on the collar which rotates freely. This assembly, therefore permits the indicator to be tightly affixed to the rotor while allowing the rotor to move freely with a blocked indicator.

(b) When the measuring head and rotor are decoupled, by pushing down on the coupling lever, the braking effect on the driving collar is mainly obtained by a spring loaded leather washer on which the rotating ring rests. The dissipation of kinetic energy of the rotor at the moment of decoupling occurs presumably in less than 0.1 sec according to manufacturing specifications.

The determination of fluid elasticity utilizes three measured quantities, viz, a speed factor U which is indirectly proportional to the angular velocity of the rotor, the elastic relaxation angle φ, and the value S_c which is proportional to the torque on the rotor. In the present studies the value of S_c was obtained independently without the EIZ attachment so that the torque measurement would not include the contribution made by the braking effect of the driving collar. The relationship between rotor torque and the measured quantity S_c can be obtained in calibration experiments as described previously[1]. The instrument constants A, B, C for the Haake Rotoviscometer tabulated in Table I are used to determine shear rate ($\dot{S}$), shear stress (σ), viscosity (η), elastic angle of deformation ($\tan \gamma$), elastic modulus of shear (G), and relaxation time (t_r) using the following relationships:

$$\text{Shear Rate} \equiv \dot{S} = B/U, \ \text{sec}^{-1}$$

$$\text{Shear Stress} \equiv \sigma = A \cdot S_c, \ \text{dynes/cm}^2$$

$$\text{Apparent Viscosity} \equiv \eta = \sigma/\dot{S}, \ \text{poise} \qquad (2)$$

$$\text{Elastic Angle of Deformation} \equiv \tan \gamma = \varphi/C$$

$$\text{Shear Modulus} \equiv G = \sigma/\tan \gamma, \ \text{dynes/cm}^2$$

$$\text{Relaxation Time} \equiv t_r = \eta/G, \ \text{sec}$$

Assuming an exponential relaxation, $1/t_r$ is the exponential rate constant.

A 100:1 gear reducer was attached between the motor drive and the flexible drive cable in order to measure the shear stress and relaxation angle at very low shear rates.

TABLE I. INSTRUMENT CONSTANTS FOR THE RV1 HAAKE ROTOVISCOMETER WITH ELZ VISCOELASTIC ATTACHMENT

Rotor	Rotor Radius (cm)	Instrument Constants		
		B (sec^{-1})	A ($dynes/cm^2$-scale div)	C
MV I	2.004	1370	32.6	2.67
MV II	1.84	520	36.7	6.7
MV III	1.52	259	53.1	13.6

MV Beaker radius is 2.10 cm; Rotor length is 6.00 cm

2.2.1 Experimental Results

The three fire retardants, Phos-Chek XA, Fire-Trol R100 and Fire-Trol R931 were prepared in the previously described manner[1], and the relaxation angles of these fluids were measured using the Haake ELZ Visco-Elastic attachment with and without the gear reducer on the motor drive. As the fluid gap between the rotor and stationary cup increases the relaxation angles increase under the same shear rate conditions. Very little elastic recovery was found in the Fire-Trol 100 retardant, as indicated by the relaxation angle measurements using rotors MV I, II and III (the gap sizes, "measuring gap" when these rotors are used are 0.096, 0.26 and 0.58 cm respectively). This confirms the initial belief that the clay thickener in Fire-Trol 100 does not confer elastic properties to the shearing liquid. On the other hand, significant angular rotor deflections were observed for Fire-Trol 931 - indicating some elastic behavior. The origin of this elasticity is not known, but is presumably due to the presence of the polyphosphate chains. Only minimal angles of recovery were observed for the Phos-Chek XA retardant with the MV I rotor; however, experimentally significant values were obtained with the smaller rotors.

The measured behavior of the elastic deformation angle as a function of shear rate for Phos-Chek and Fire-Trol 931 are shown in Figures 2 and 3. It was observed that the deformation angle increases with shear rate for both fire retardants, and then levels off at relatively high shear rates. When the relaxation times, t_r, are computed directly from these data,

$$t_r = \varphi \cdot U/BC \qquad (3)$$

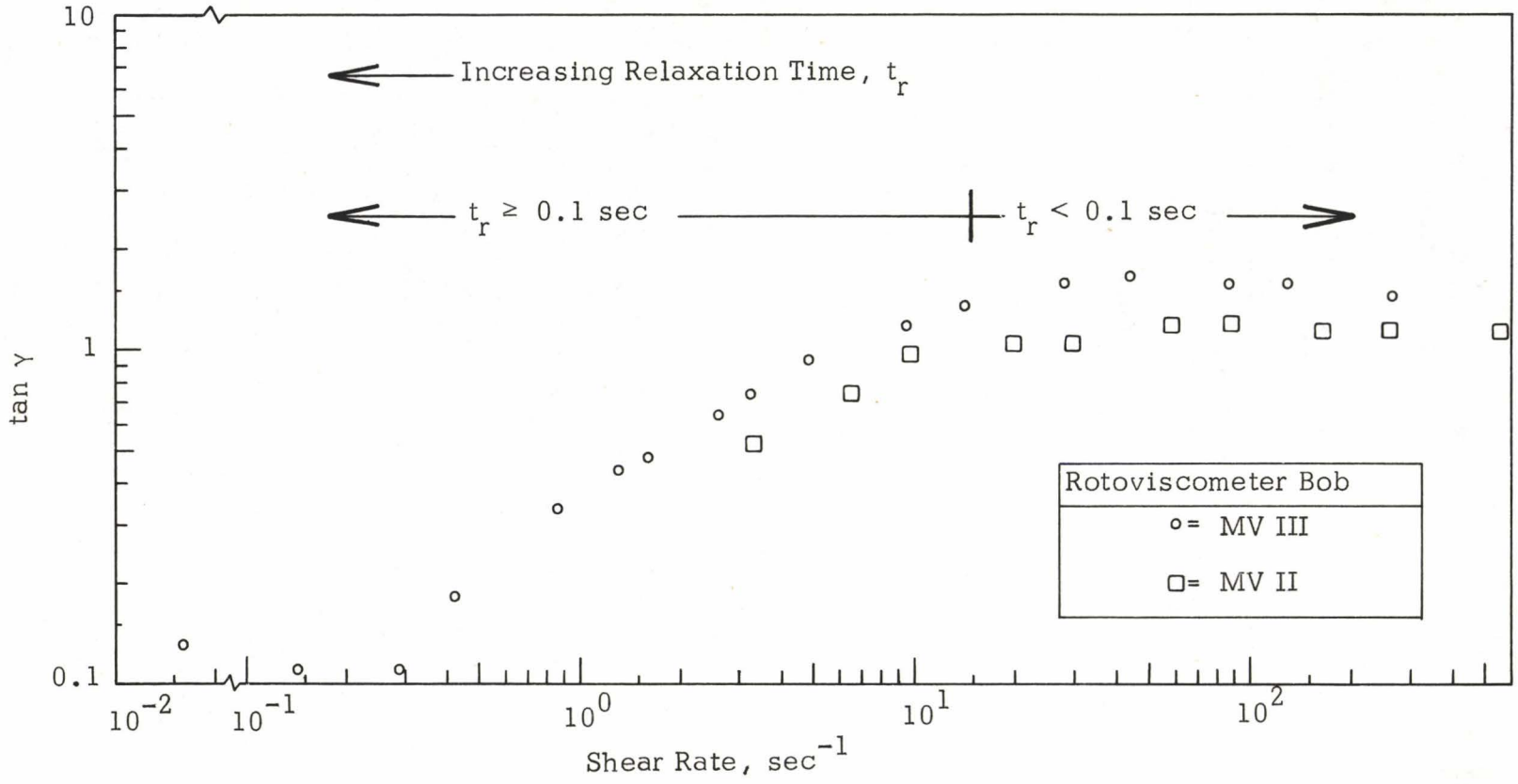

Figure 2. Measured Elastic Deformation Angle (γ) of Phos-Chek XA vs Shear Rate at 20°C.

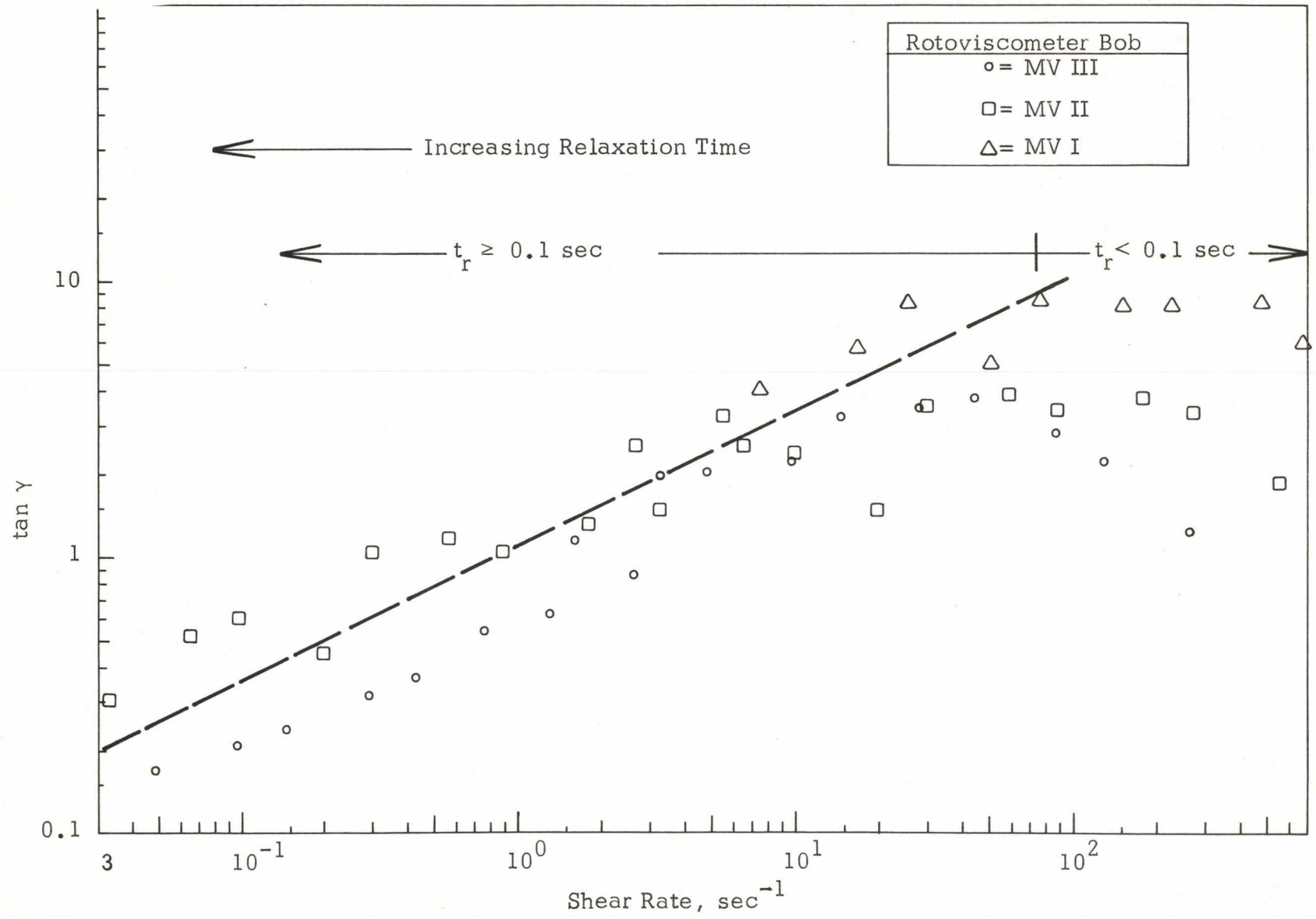

Figure 3. Measured Elastic Deformation Angle (γ) of Fire-Trol 931 vs Shear Rate at 20°C.

Thus t_r is directly proportional to the measured recovery angle. It was noticed that the deformation angles level off with shear rate when the estimated relaxation times approach, downward, a value of about 0.1 sec. These observations and the fact that the dissipation of kinetic energy after the measuring head is decoupled from the rotor occurs in a time period close to 0.1 sec indicated that the data obtained in the shear rate regime where the estimated elastic deformation angles level off cannot be used, and that under these estimated relaxation time conditions the instrument should not be employed for the determination of recovery angle. It has been found in the literature that there are at least two studies in which these types of measurements have been made under these undesirable conditions.

An additional factor limits the use of this data for the estimate of elastic shear modulus and recoverable shear at low shear rates. Thus although recovery angles could be measured at low shear rates, the correspondingly low torques on the rotor at these rates in some cases could not be measured because they were below the detection limits of the instrument.

The elastic strain (recoverable shear, s) was computed as a function of shear rate from the experimental data by the equation

$$s = \eta \dot{S}/G \qquad (4)$$

where the values of η and G both depend on $\dot{S}$. The Krieger-Maron-Elrod treatment was used to correct the shear stress data[1], and for estimating the stress distribution within the fluid gap between rotor and cup. From the corrected values, the viscosity and shear modulus were estimated at each shear rate condition.

The estimated values of recoverable shear, s, as a function of shear rate, for Phos-Chek and Fire-Trol 931 are shown in Figures 4 and 5. The values of s obtained previously from the capillary tube measurements for Phos-Chek XA[1] are included for comparison with the data obtained from the present coaxial cylinder measurements. An extrapolation shows good agreement between the two sets of data, except for the smallest value of s obtained by the capillary tube technique where the experimental error was large - due to the nature of the technique. The overall linear logarithmic elastic behavior of Phos-Chek given by the data in Figure 4 is therefore assumed to be an improvement over the general behavior given by the more-limited data in ref. 1.

Although the logarithmic plot of s vs $\dot{S}$ for Phos-Chek was linear, the corresponding plot for Fire-Trol 931 exhibits curvature. The assumed extrapolation of the experimental data points is shown in Figure 5. However it is possible that the curvature becomes more pronounced so that the value of s at the higher shear rates is less than that shown by the assumed extrapolation.

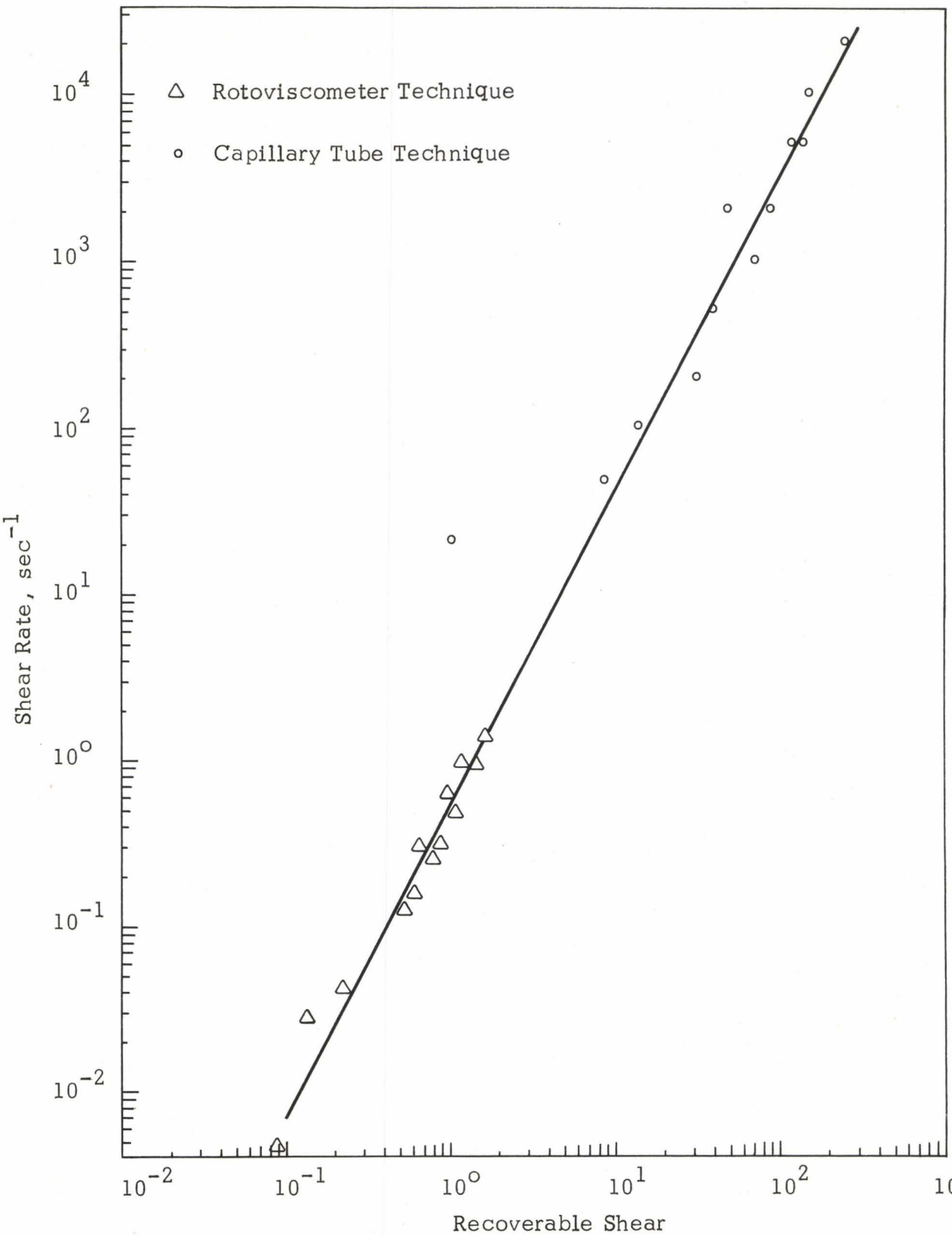

Figure 4. Recoverable Shear vs Shear Rate for Phos-Chek XA at 20°C.

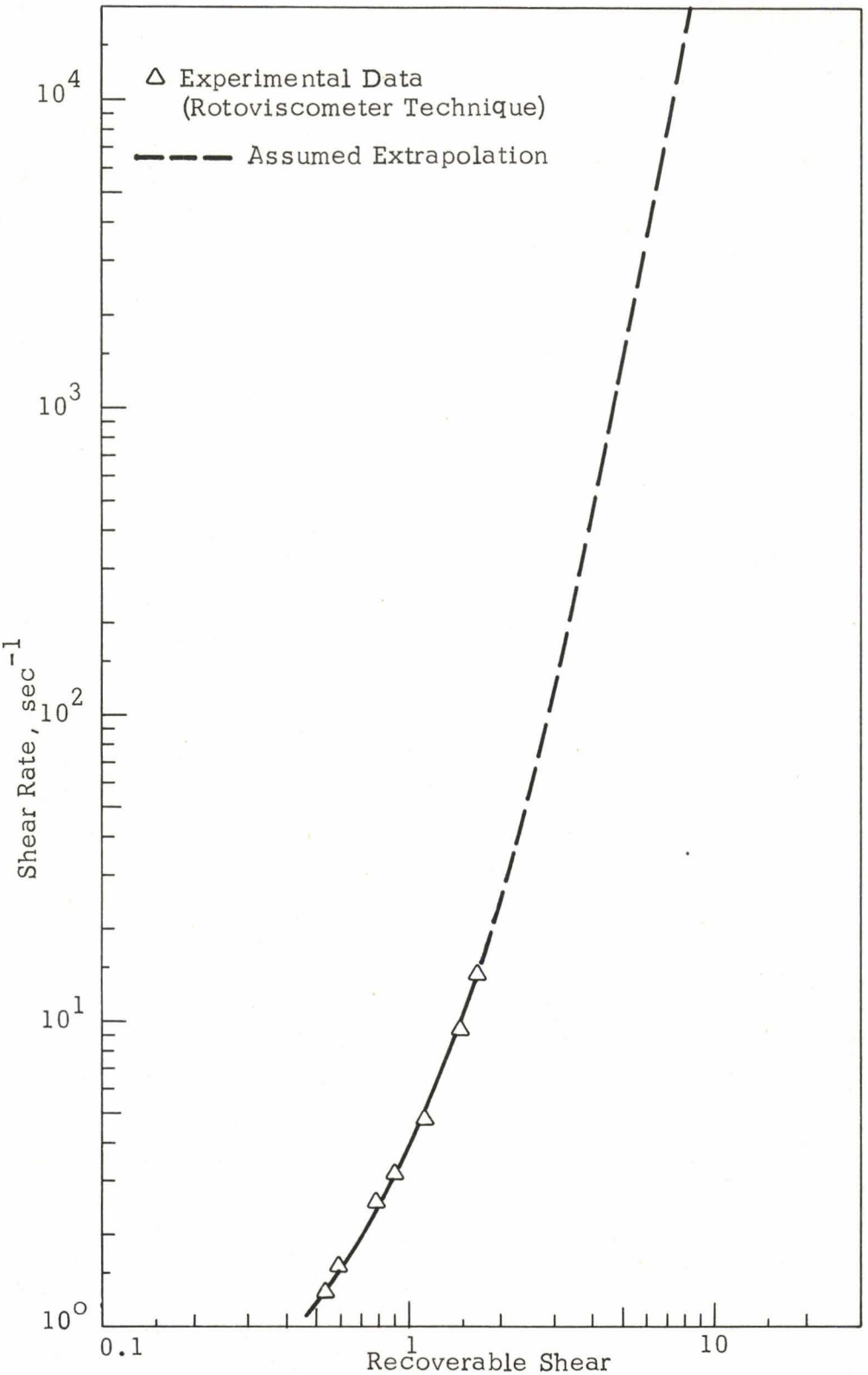

Figure 5. Estimated Recoverable Shear vs Shear Rate for Fire-Trol 931 at 20°C.

2.2.2 Effective Viscosity

The values of s given in Figures 4 and 5 were combined with the apparent viscosities determined previously[1] to give the effective viscosity, η_e, of Phos-Chek XA and Fire-Trol 931, as defined in Eq. (1). A plot of η_e vs shear rate for these two retardants is given in Figure 6. Since Fire-Trol 100 is nonelastic, its apparent viscosity curve (determined previously[1]) also defines its effective viscosity behavior, and this curve is also shown in the figure. It will be observed from Figure 6 that at very low shear rates ($\sim 1\ sec^{-1}$) the effective viscosity of Fire-Trol 100 is the largest of the three retardants, followed by Phos-Chek and then Fire-Trol 931. As the shear rate is increased however, the effective viscosity of Fire-Trol 100 is reduced rapidly - due to shear thinning - whereas elasticity retards the reduction of the effective viscosity in Phos-Chek. The result is that at the higher shear rates experienced by the liquids during their aerodynamic breakup, the effective viscosity of Phos-Chek is much larger than that of the two Fire-Trol solutions, and consequently its droplet size is larger.

Although the apparent viscosity of Fire-Trol 931 is much smaller than that of Fire-Trol 100 at low shear rates, as the shear rate is increased the effective viscosity of Fire-Trol 100 is reduced rapidly while that of Fire-Trol 931 reduces more slowly - due to its elastic nature. At a sufficiently large shear rate ($400\ sec^{-1}$) the effective viscosities of the two retardants become equal, and at larger shear rates the effective viscosity of Fire-Trol 931 is greater than that of Fire-Trol 100.

The results of the present studies show that Phos-Chek is more elastic at the lower shear rates than determined previously[1], and that Fire-Trol 931 also exhibits some elastic behavior under shear - in opposition to the previous conjectures. Fire-Trol 100 is nonelastic - in agreement with previous conclusions. Consequently the effective viscosity vs shear rate expression obtained previously for Fire-Trol 100 remains the same, whereas that for Phos-Chek and Fire-Trol 931 are modified to some extent. The most significant overall result of these modifications is that the aerodynamic breakup characteristics and terminal particle size of the two Fire-Trol retardants will be more nearly the same than estimated previously. Further discussion regarding the breakup behavior of the retardants will be given subsequently.

2.2.2.1 Analytical Expressions of Effective Viscosity

A least squares fit was made of the effective viscosity vs shear rate curves given in Figure 6, resulting in the following empirical equations for the retardants.

Phos-Chek XA $(1 \le \dot{S} \le 2(10^5) sec^{-1})$

$$\eta_e = 84.19 - 70.43 \log \dot{S} + 29.3(\log \dot{S})^2 - 6.991(\log \dot{S})^3 + 0.943(\log \dot{S})^4 - 0.0528(\log \dot{S})^5 \quad (5)$$

Fire-Trol 100 $(10 \le \dot{S} \le 6(10^4) sec^{-1})$

$$\log \eta_e = 2.033 - 0.5089 \log \dot{S} - 0.2292(\log \dot{S})^2 + 0.03937(\log \dot{S})^3 \quad (6)$$

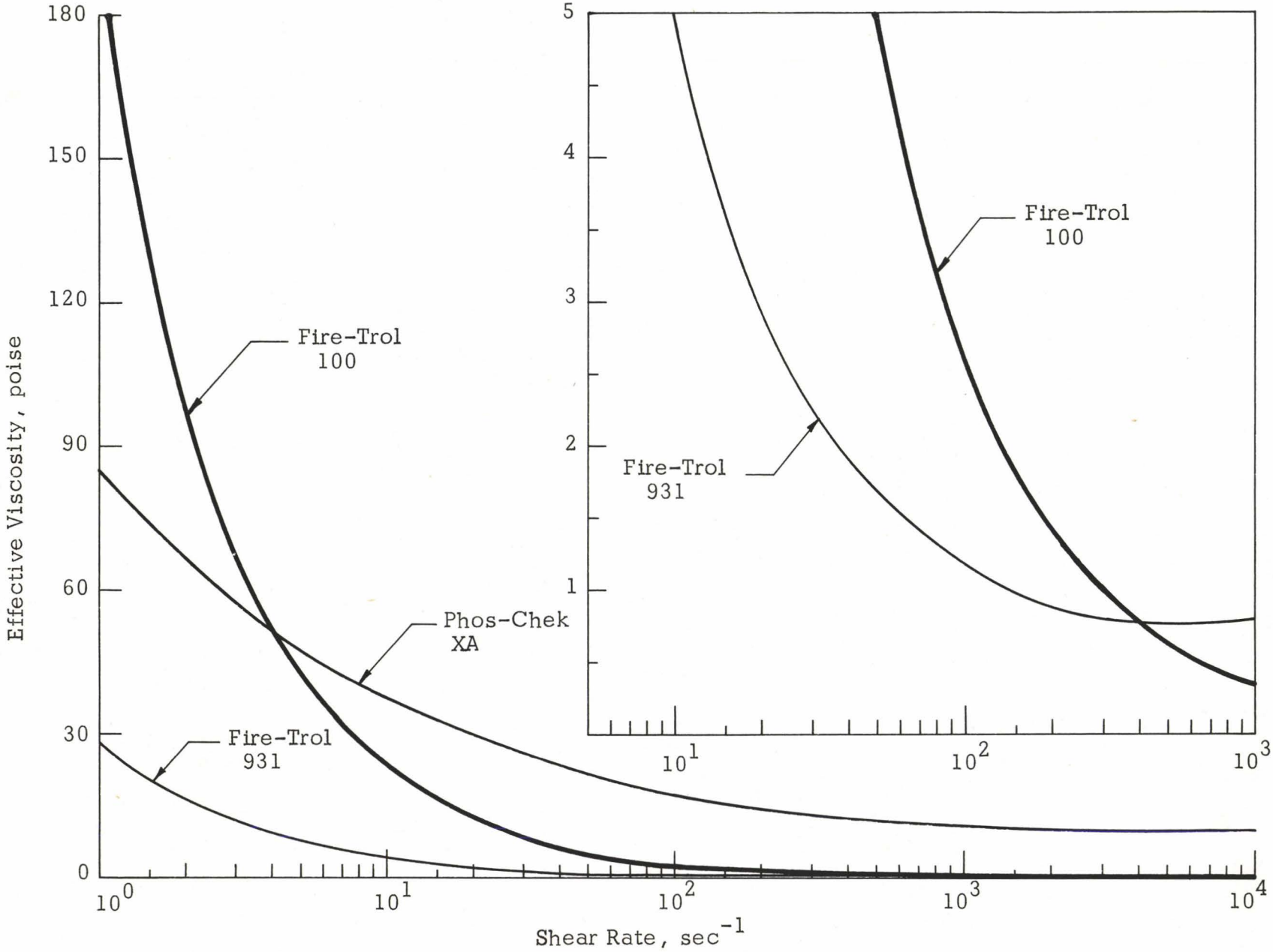

Figure 6. Effective Viscosity of the Fire Retardant Solutions as a Function of Shear Rate.

$$(1 \leq \dot{S} \leq 10 \text{ sec}^{-1})$$

$$\eta_e = 184\ \dot{S}^{-0.746} \tag{7}$$

Fire-Trol 931 $(1 \leq \dot{S} \leq 10^5 \text{ sec}^{-1})$

$$\eta_e = 28.01 - 51.71 \log \dot{S} + 47.17(\log \dot{S})^2 - 25.38(\log \dot{S})^3 + 7.974(\log \dot{S})^4 - 1.323(\log \dot{S})^5 + 0.0879(\log \dot{S})^6 \tag{8}$$

In the preceding equations, η_e is in poise, $\dot{S}$ is in sec^{-1}, and log is common logarithm.

2.3 YIELD STRESS MEASUREMENTS

Each of the fire-retardant solutions, Phos-Chek XA, Fire-Trol 100, and Fire-Trol 931 have been found to obey the power-law relationship between shear stress (and apparent viscosity) and shear rate. That is, the graphical plots of log σ (and log η) vs log $\dot{S}$ are linear. Linearity occurs over a relatively broad range of shear rates for Phos-Chek XA and Fire-Trol 100, and over a lesser shear rate range for Fire-Trol 931. At low shear rates the deviations from linearity which occur for all three retardants have been assumed to be indications of "plug flow". This condition occurs when the shear stress, σ_r, within the gap between the rotating bob and stationary cup falls below the yield stress, Y. Between the stationary cup and the radial distance, r, where $\sigma_r < Y$ there should exist a non-moving body of material, i.e., the "plug", while across the remaining gap from r to the moving bob where the stress exceeds the yield value the material exhibits laminar flow. When plug flow within the measuring gap occurs it has the effect of narrowing the effective gap width. This occurrence causes a deviation in the power-law relationship, resulting in a change in the power-law slope, n.

As previously discussed, transitions in the slopes of the log-log plots of shear stress vs shear rate for the three fire retardants under study were observed. These transitions were sharp enough to allow the estimation of yield stresses, as shown in Figure 7a. The values previously estimated for Phos-Chek XA, Fire-Trol 100 and Fire-Trol 931 at 20°C were 188, 235 and 20 dynes/cm^2 respectively, using the corrected data obtained from the Rotovisco instrument with the largest (MVI) bob over a shear rate range of 8.5 to 1370 sec^{-1}. On the present program, additional measurements of yield stress were made using improved techniques for comparison with these values. These techniques involved

(a) the employment of a 100:1 gear reduction attachment to the Rotovisco instrument which permits shear stress measurements at shear rate as low as 10^{-3} sec^{-1}, and

(b) stress relaxation measurements.

2.3.1 Experimental Results (Inclusion of Low Shear Rate Data)

Since the non-linearity in the log-log plots of shear stress versus shear rate occurs at low shear rates, e.g. < 30 sec^{-1} for the fire retardants under study, the capability of extending the measurements to shear rates below that permitted by the standard gear drive of the Rotovisco instrument can result in more confident estimates of the origin of plug flow. Using this more sensitive approach a yield stress for Phos-Chek XA of 165 dynes/cm^2 was estimated. This value is slightly lower than that previously estimated (185 dynes/cm^2) but still within the range of values, 124-182 dynes/cm^2, estimated by interpreting the previous data using the Reiner-Rivlin model for a Bingham body.

Similarly, a yield stress value of 200 dynes/cm^2 was obtained for Fire-Trol 100 from data obtained over this wider shear rate range. This estimate compares with a previous value of 235 dynes/cm^2 and a range between 181-199 dynes/cm^2 using the Reiner-Rivlin model. The shear stresses in Fire-Trol 931 at low shear rates are much lower than those in the more viscous retardants. At the lower shear rates obtainable with the gear reduction attachment the shear stresses in Fire-Trol 931 were below the detection limits of the instruments. Therefore no additional estimates of yield stress for this retardant could be made.

These new data were obtained using the MVI rotor. The measuring gap width which is 0.096 cm is the narrowest possible with the MV beaker and the most sensitive to the detection of plug formation.

2.3.2 Observations of Stress Relaxation

The relaxation of stress in the fire retardant suspensions was dynamically observed in an attempt to independently estimate the exponential rate constant, t_r (Eq. 2,3), for stress relaxation

$$\sigma(t) = \sigma_o \exp(-t/t_r) \qquad (9)$$

where σ_o is the shear stress during constant shear and $\sigma(t)$ is the shear stress at time, t, after shearing is terminated. The time constants for recovery for the three fire retardants were found to be comparable or shorter than the time response characteristics of the recording instrumentation employed. However it was observed that complete relaxation does not always occur in Fire-Trol 100. Instead, a reproducible transition between partial and complete stress recovery occurs, as illustrated in Figure 7b. This transition was found to occur at a shear rate of 43.2 sec^{-1}, with a measuring gap of 0.58 cm. The shear stress across the measuring gap was estimated to be between 254 and

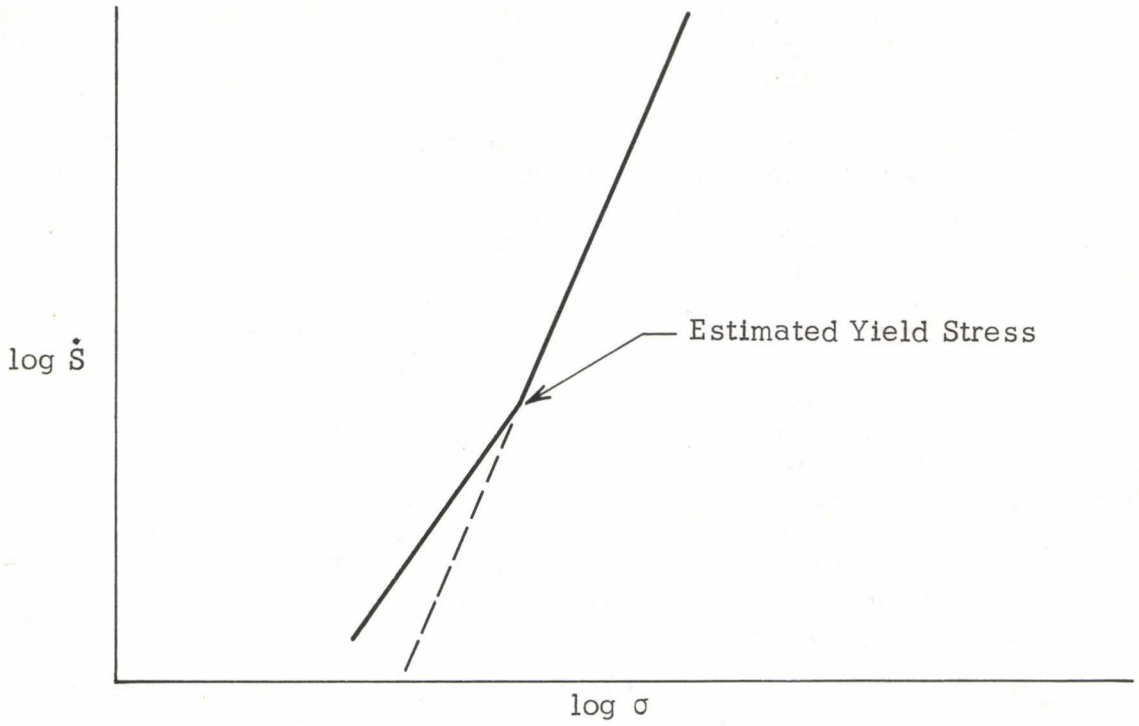

(a) Estimation of Yield Stress Using Power-Law Relationship Between Shear Stress and Shear Rate.

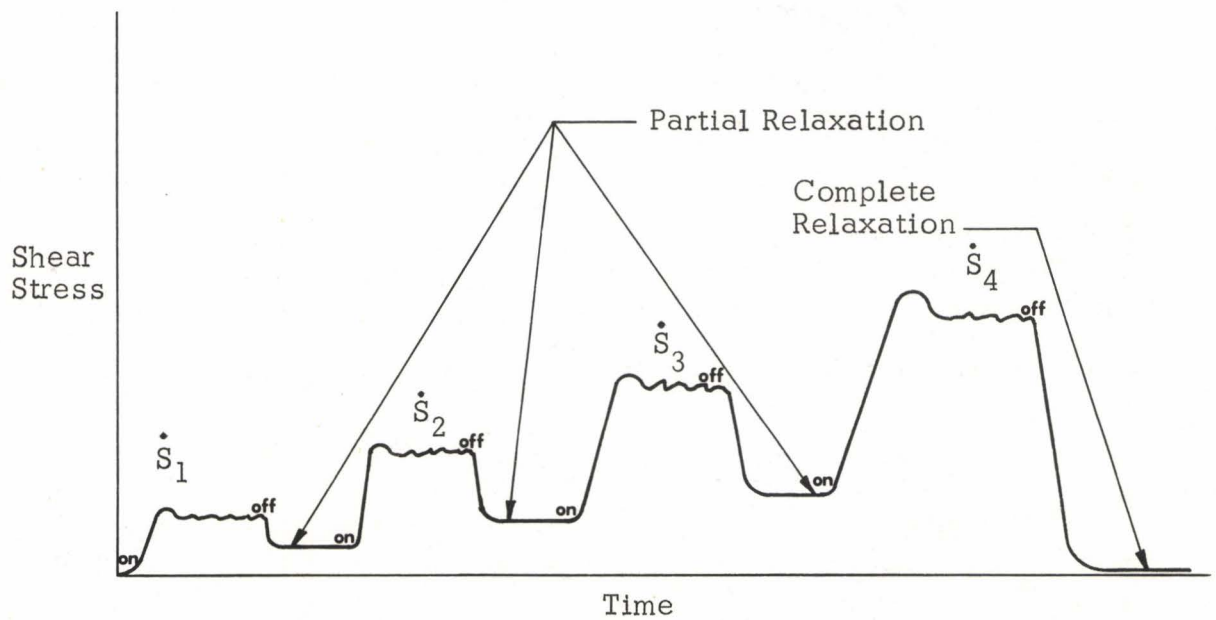

(b) On-Off Technique for Measuring Yield Stress. (Progressively larger shear rates, $\dot{S}$, applied to fluid, in steps, until fluid completely relaxes when shearing is abruptly terminated)

Figure 7. Methods Employed for the Estimation of Yield Stress.

133 dynes/cm^2 based on the measured rotor torque. These values represent the estimated shear stresses at, respectively, the rotor bob- fluid and the fluid- stationary cup wall interfaces according to the Krieger-Maron model.

It is postulated from these observations that complete stress relaxation in Fire-Trol 100 occurs only when the yield stress is exceeded within the gap. The value of 254 dynes/cm^2 is thus considered to be an upper limit of the yield for Fire-Trol 100.

3. EXTENDED LIQUID BREAKUP ANALYSIS AND CORRELATION

As discussed in ref. 1, as bulk liquid fire retardant is released from an aircraft the liquid initially undergoes wind stripping (surface erosion) at its exposed surfaces into small particles (droplets). Simultaneously the bulk liquid undergoes deformation (thinning and lateral spreading) by aerodynamic forces, followed by breakup by Taylor instability growth into many individual particles - which may subsequently undergo further breakup by either surface erosion or bag formation. In ref 1, models were developed for describing the breakup of the liquid by both Taylor instability growth and surface erosion, and estimates were made of the breakup characteristics under various conditions and the effects of the important system parameters and fluid properties on the breakup characteristics. In this section further analysis and discussion is presented of the aerodynamic breakup, dispersion and settling properties of the retardants, and the factors that control the ground pattern concentration.

3.1 TERMINAL DROPLET SIZE PRODUCED BY INITIAL PERIPHERAL WIND STRIPPING

As the bulk liquid retardant is released from the aircraft it initially undergoes peripheral wind stripping (surface erosion) at its exposed surfaces into small droplets. The resulting ground concentration of retardant is generally much smaller than that necessary for effective fire control, and is not usually considered as forming part of the meaningful pattern of the dispersed retardant.[2] Nevertheless it is useful to estimate the droplet sizes produced since the treatment illustrates various factors of importance in understanding liquid breakup. An eventual experimental determination of droplet size in this region could thus help check the general validity of the surface erosions model that is used to predict terminal droplet size throughout the effective ground pattern.

3.1.1 Number Distribution of Droplets

The number formation rate of droplets that are wind stripped (eroded) from a unit surface area of liquid is given by Eq. 13-14 of ref. 1. Using the new effective viscosity equations given in Eq. 5-8 of this report in the solution of these equations gives the calculated size distribution curves for the three retardants and water shown in Figure 8 for an aircraft velocity of 100 knots. Note that these distribution curves are based on the number of particles stripped from the surface, and not the particle mass. In performing these computations the droplet formation rate was computed over a number of wavelength increments - starting from the minimum wavelength - and the computations terminated when the number contribution from a new increment was less

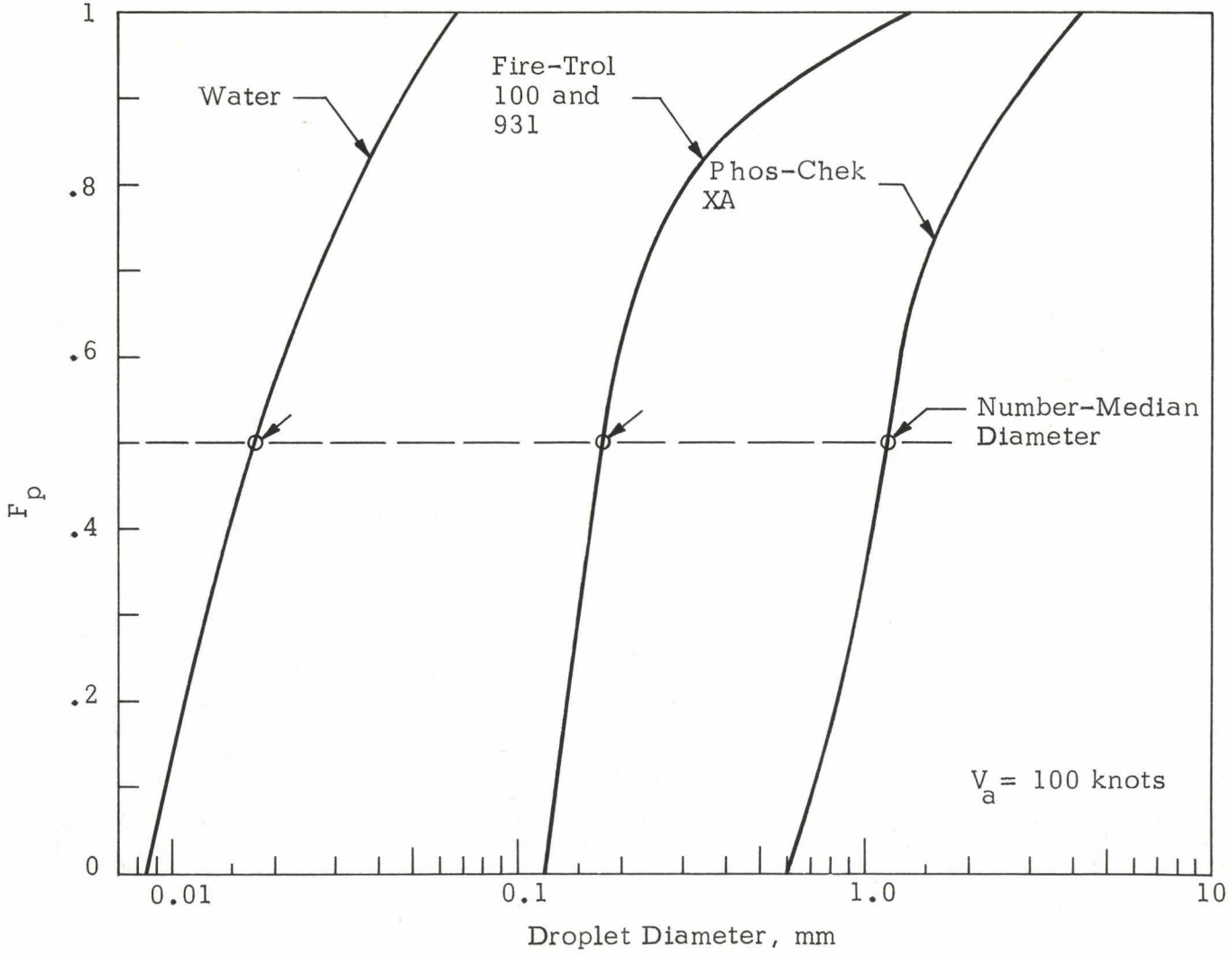

Figure 8. Computed Size Distribution of the Droplets Produced by the Initial Peripheral Stripping of the Liquid Fire Retardants. F_p is the Cumulative Fraction of the Number of Liquid Particles.

than about 0.005 of the total cumulated droplet formation rate at that point of the calculation. Further comments regarding the calculations and their results will be given subsequently.

3.1.2 Mass Distribution of Droplets

The mass formation rate of the eroded droplets is given by Eq. 20-21 of ref. 1. The results of the computations for the mass distribution of the eroded droplets using the new effective viscosity equations are shown in Figure 9. These computations were performed in the same general manner as for number formation, and the same maximum wavelength cutoff point was also used.

A comparison of Figures 8 and 9 shows that for any retardant the cumulative fraction of particles increases more rapidly with increasing particle size than the cumulative fraction of mass at the smaller droplet diameters, whereas the opposite is true at the higher droplet diameters. This results because in general the formation rate of small droplets is faster than that of large droplets, but large droplets contain more mass. It will also be observed that the mass median droplet diameter is larger by a small factor (2.4-5) than the number median diameter, and this also results because small particles contain little mass. The mass distribution is consequently usually of much more practical utility than the number distribution.

In Table VI and Figures 44,45 of ref. 1 a preliminary estimate was made of the terminal particle size distribution of the aerially delivered retardants, using the Mayer equation to determine the mean droplet size and the empirical log normal distribution function to determine the size distribution. Since the wind velocity used in the calculations was the aircraft velocity, the preceding calculations actually apply more accurately to the initial peripheral wind stripping region presently under consideration than to the main (Taylor instability) breakup region to be discussed subsequently. In view of the nature of the preceding calculations, the results are of interest for comparison with the present results.

The computed mass mean droplet diameter of Phos-Chek using the present computational method and new effective viscosity curve is 3.0 mm - in good agreement with the previous value (3.3 mm). The shear rate and effective viscosity during breakup are roughly 853 sec^{-1} and 11.4 poise. The new effective viscosity curve is approximately the same as the previous curve in this shear rate range and hence has little effect on the results.

The effective viscosity curve of Fire-Trol 100 is the same as used previously, and the present computed mean droplet diameter of 0.9 mm is slightly larger than that computed before (0.54 mm). Some of this difference may be due to a slight error in the preceding computer program since the new value for water ($4.24(10^{-2})$ mm) is also roughly the same as before ($3.8(10^{-2})$). The shear rate and effective viscosity of these liquids during breakup are 582 and 1290 sec^{-1}, and 0.54 and 0.0087 poise, respectively.

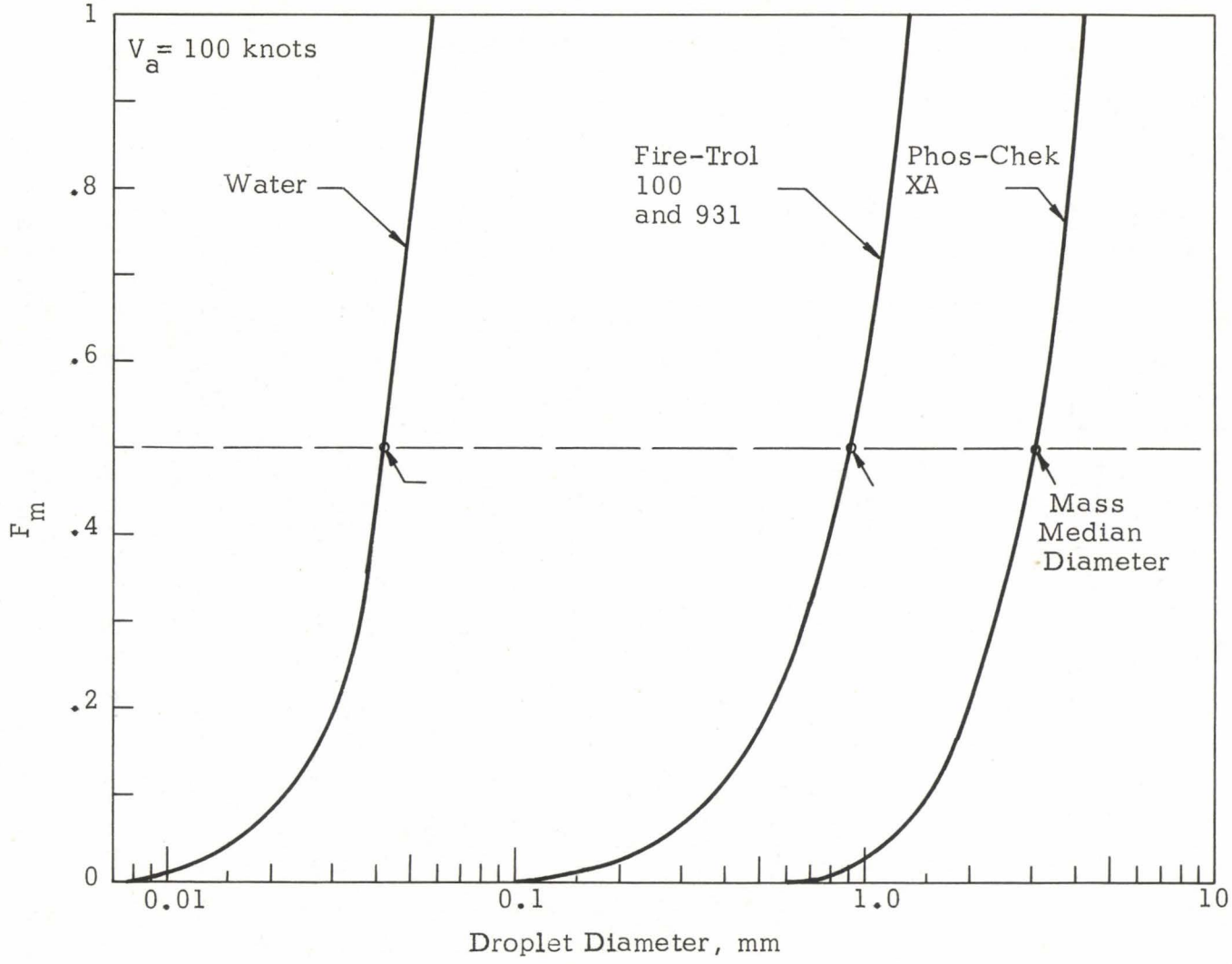

Figure 9. Computed Size Distribution of the Droplets Produced by the Initial Peripheral Stripping of the Liquid Fire Retardants. F_m is the Cumulative Fraction of the Mass of the Liquid Particles.

The effective viscosity of Fire-Trol 100 and 931 are roughly the same in the shear rate range where the initial peripheral stripping (at V_a = 100 knots) occurs, as may be seen in Figure 6. Assuming that the extrapolated curve in Figure 5 - on which the Fire-Trol 931 curve in Figure 6 is based - is correct, the estimated droplet size of Fire-Trol 931 is roughly 9% greater than that of Fire-Trol 100. On the other hand it is just as likely that the effective viscosity is overestimated slightly at high shear rates - as discussed previously. This could decrease the droplet size of FT 931 slightly below that of FT 100. Thus to the present accuracy the droplet sizes of the two Fire-Trol retardants in the initial peripheral stripping region are estimated to be roughly the same - as shown in the figures.

3.1.2.1 Comparison With the Log Normal Distribution

It is of interest to compare the particle mass distribution curves computed on the present program - which are based on the Mayer surface erosion model - with the previously computed curves[1] based on the empirical log normal probability distribution function. The comparison is shown in Figure 10. It may be seen that within the accuracy of both computations that both methods are in reasonable agreement for the first 90-95% of the cumulated mass. However the log normal distribution function predicts that a small percentage (5-10%) of the mass is much larger than that estimated from the surface erosion model. The general validity of this prediction is not known but seems reasonable on the basis of existing experimental data on the breakup of small drops and jets. It is believed that the discrepancy between the two calculations at large particle sizes is due to the somewhat arbitrary scheme used to determine the maximum wavelength (and hence particle size) in the Mayer distribution function. The cutoff scheme used has negligible effect on number distribution, but can be of more consequence on mass distribution since a very few large droplets can possess more mass than many smaller droplets.

It is therefore tentatively concluded that the method used earlier in ref. 1 is just as reliable - and possibly even more accurate - than the present method of using the entire droplet size distribution function to calculate the droplet mass distribution. The earlier method consisted of computing the mean droplet size from the Mayer equation - using the effective viscosity expression - and estimating the size distribution by the log normal probability equation. This procedure is recommended for future studies in view of the complexities of using the distribution functions based on the Mayer equation.

3.1.3 Relative Rates of Liquid Stripping

The wind stripping of a liquid surface removes droplets from the surface, and the rate of removal depends on the liquid properties and the wind velocity. The results of the computations on which Figure 8 is based gives a number that is proportional to the number of droplets formed per unit surface area per second for the various retardants. The computed values for Phos-Chek, the Fire-Trols and water are $3.5(10^3)$, $1.3(10^4)$ and $4(10^6)$, respectively. The droplet removal rate from water is thus about a thousand times faster than that from Phos-Chek and 300 times faster than that from the Fire-Trol retardants.

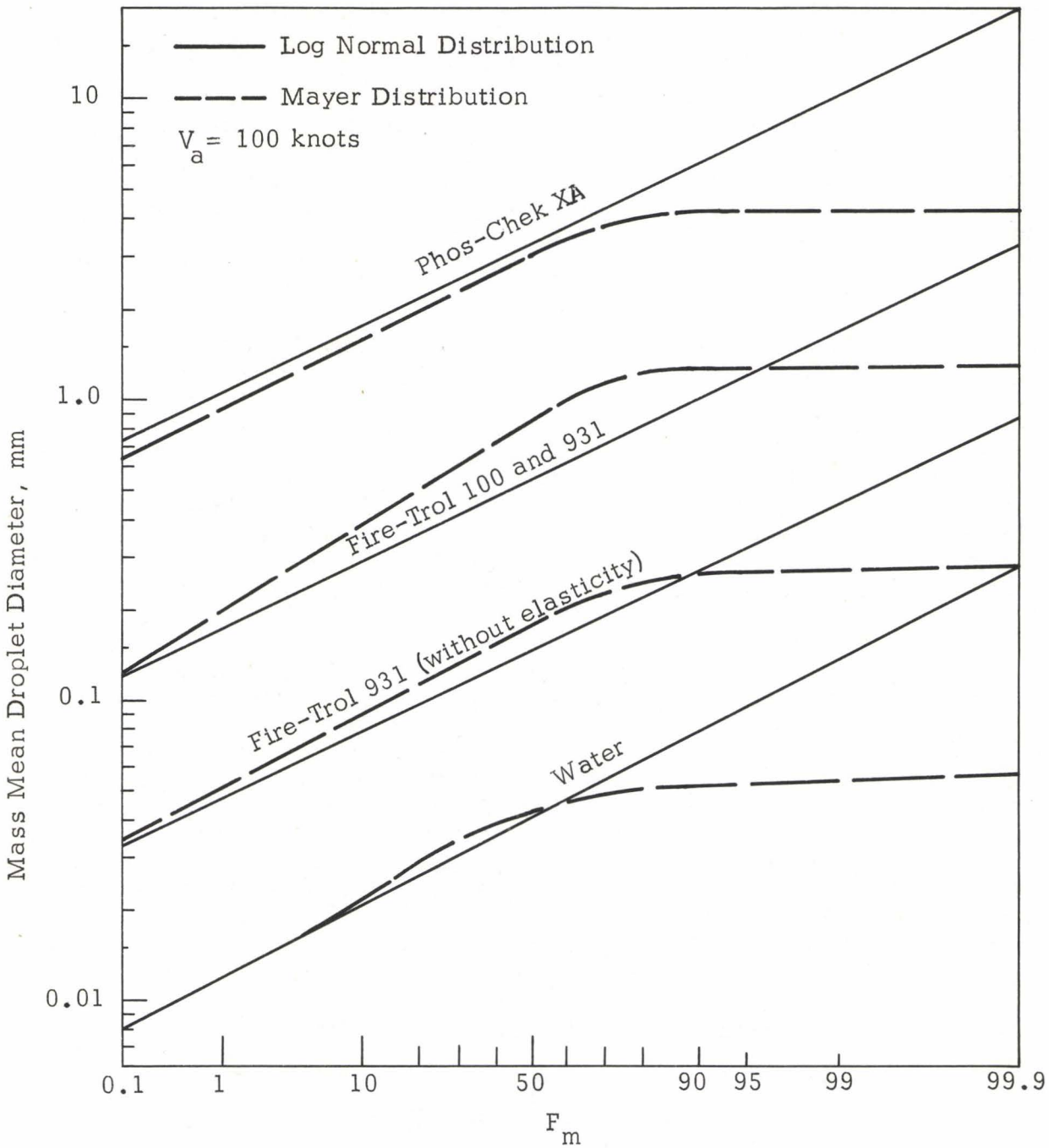

Figure 10. Comparison of the Initial Droplet Size Distribution Computed Using the Log Normal and Mayer Distribution Functions. F_m is the Cumulative Percentage of Liquid Mass.

On the other hand the size of the Phos-Chek droplets is larger than that of water and the Fire-Trols. The results of the computations on which Figure 9 is based gives a number that is proportional to the number of grams of droplets formed per unit surface area per second. The values for Phos-Chek, the Fire-Trols and water are $1.7(10^4)$, $4.3(10^3)$ and $12.(10^3)$, respectively. These values are subjected to some uncertainty - related to the wavelength cutoff criterion discussed previously. However they demonstrate that although the initial droplet removal rate from Phos-Chek is small compared with that of water and the Fire-Trols, the total mass removal rate (per unit area) may be comparable or actually larger since the removed droplets are larger. This conclusion seems somewhat surprising at first, but appears to be well-founded from fundamental considerations.

3.2 TERMINAL DROPLET SIZE PRODUCED IN THE EFFECTIVE GROUND PATTERN

During the initial peripheral stripping of an aerially-delivered falling liquid retardant (which was just discussed), the liquid simultaneously undergoes deformation (thinning and lateral spreading) - followed by breakup into many particles by Taylor instability growth. The nature of the deformation and Taylor instability breakup processes was discussed previously.[1] Subsequent to the Taylor breakup of the liquid, many of the individual particles produced may undergo further breakup by either surface erosion (wind stripping) or bag formation.

In ref. 1 a preliminary estimate was made of the terminal droplet size of the retardants, based on the assumption that the particles produced by Taylor instability breakup undergo further breakup by surface erosion. However as mentioned previously, it is now believed that this estimate applies more accurately to the droplets produced by the initial peripheral wind stripping of the liquid prior to Taylor breakup, since the wind velicity was assumed to be the full aircraft velocity. In actuality however the liquid velocity is slowed down significantly by air drag during the Taylor instability breakup process, and it is necessary to use the reduced wind velocity in estimating terminal droplet size. The general effect of reduced wind velocity is to increase the terminal droplet diameter above that computed previously on the basis of the aircraft velocity.

3.2.1 Liquid Velocity Reduction by Air Drag

The velocity, V, at time t_i of a liquid with mass, m, and cross-sectional area, A, moving through still air and subject to air drag is given by

$$V = \frac{V_a}{KV_a t_i + 1} \tag{10}$$

$$K = \rho C_d A/2m \tag{11}$$

where V_a is the initial velocity of the liquid at zero time, ρ is air density, and C_d is the drag coefficient. In using this equation to estimate the velocity of the liquid particles just subsequent to the Taylor instability breakup of the aerially-delivered liquid, the following considerations apply.

Subsequent to its release from the aircraft the liquid is subjected to air drag and undergoes deformation followed by Taylor instability breakup. The total breakup time, t_b, is given by Eq. (45) of ref. 1, i.e.,

$$t_b = t_d + t_i \tag{12}$$

where t_d is the deformation time of the bulk liquid, and t_i is the effective time for the liquid to undergo breakup by Taylor instability growth subsequent to its deformation. The solution of this equation was discussed previously.[1] The initial effect of the air drag on the released liquid is to deform the liquid - which results in its thinning and lateral spreading. During this phase the horizontal velocity of the free falling liquid is essentially the same as that of the aircraft. At the end of deformation, however, the air drag causes Taylor instability growth in the liquid and simultaneously retards its velocity so that the velocity of the liquid rapidly drops below the aircraft speed. The time that the air drag acts to slow the liquid is the time required for the deformed liquid to undergo breakup by Taylor instability growth. Thus the value of t_i in the drag equation, i.e., Eq. (10), is equal to the Taylor instability breakup time t_i, in Eq. (12). Likewise the value of A in Eq. (11) is determined by the effective radius, R_e, of the deformed liquid when Taylor breakup occurs, i.e., $A = \pi R_e^2$. The evaluation of R_e was discussed previously.[1] Also, $m = \rho_l V_o$, where ρ_l is liquid density and V_o is the retardant tank volume, and V_a is the aircraft velocity. The drag parameter, K, then becomes

$$K = \frac{\rho C_d \pi R_e^2}{2\rho_l V_o} \tag{13}$$

3.2.2 Evaluation of Velocity Reduction

In evaluating the velocity reduction of the liquid during its Taylor instability breakup, information is required regarding the value of t_i in Eq. (10). This parameter is obtained in the solution of Eq. (12), and a variety of solutions were summarized in terms of t_b in ref. 1. An examination of these solutions shows that to reasonably good approximation over a wide variety of conditions

$$t_i \simeq 0.19\, t_b \tag{14}$$

This value applies for the case of $C_d = 3.5$, which is also the value selected for use in the equations.

TABLE II. COMPUTED EFFECT OF SYSTEM PARAMETERS ON THE VELOCITY REDUCTION OF LIQUID RETARDANTS WHILE UNDERGOING BREAKUP BY TAYLOR INSTABILITY.

V_a (knots)	V_o (gal)	R_o (cm)	L_o (cm)	R_e/R_o	t_i (sec)	V (knots)	V/V_a
75	700	73.8	155	4.70	0.40	52	0.70
100	700	73.8	155	4.70	0.30	70	0.70
150	700	73.8	155	4.70	0.20	105	0.70
75	1400	104.2	155	4.70	0.42	51	0.68
100	1400	104.2	155	4.70	0.32	69	0.69
150	1400	104.2	155	4.70	0.21	103	0.69
100	669	91.5	100	3.85	0.21	76	0.76
100	1338	91.5	200	5.70	0.40	59	0.59
100	2007	91.5	300	7.25	0.61	47	0.47
100	2676	91.5	400	8.55	0.82	39	0.39
100	2000	162	91.5	3.50	0.25	75	0.75
100	2000	126	153	4.90	0.33	66	0.66
100	2000	106	214	5.95	0.43	58	0.58
100	2000	93.9	274	6.86	0.56	51	0.51
100	2000	84.8	335	7.70	0.69	45	0.45

An evaluation of Eq (10) in terms of the various system parameters that enter the equation shows that for retardant tank lengths less than about 160 cm, the value of V/V_a is relatively constant and equal to a value of about 0.69 (see Table II). That is, for tank lengths of less than about 160 cm, the velocity, V, of the liquid particles produced by Taylor breakup is about 0.69 V_a, independent of tank radius, retardant composition, and aircraft velocity. For longer tank lengths the liquid velocity becomes a smaller fraction of the aircraft velocity, as shown in the table. The general effect of decreasing liquid velocity is to increase the terminal droplet size.

3.2.3 Average Terminal Droplet Size

Using the preceding generalizations regarding the reduction in liquid velocity during Taylor breakup, the mass median diameter of the droplets produced in the effective ground pattern by the CL 215 aircraft have been computed by the method used in ref. 1, i.e., using the mean diameter equation of Mayer, but using the new effective viscosity equations and reduced wind velocity. The results are shown as a function of aircraft velocity in Table III and Figure 11. Also given in the table are the shear rate and effective viscosity during breakup.

TABLE III. COMPUTED FINAL AVERAGE DROPLET SIZES IN THE EFFECTIVE GROUND PATTERN*

Liquid Retardant	Aircraft Velocity, V_a (knots)	$\dot{S}$ (sec^{-1})	η_e (poise)	d_m (mm)
Phos-Chek	75	257	13.5	10.3
	100	552	12	6.45
XA	150	1025	11	3.56
Fire-Trol	75	203	1.4	2.83
	100	378	0.81	1.33
100	150	722	0.44	0.52
Fire-Trol	75	231	0.84	1.93
	100	409	0.77	1.25
931	150	1010	0.79	0.64
	75	437	0.0087	0.092
Water	100	735	0.0087	0.063
	150	1354	0.0087	0.037

*These computed values apply to the CL-215 aircraft and in general to any retardant tank less than about 160 cm in length. For greater tank lengths the estimated mean droplet size will be slightly larger, and increases with increase in tank length.

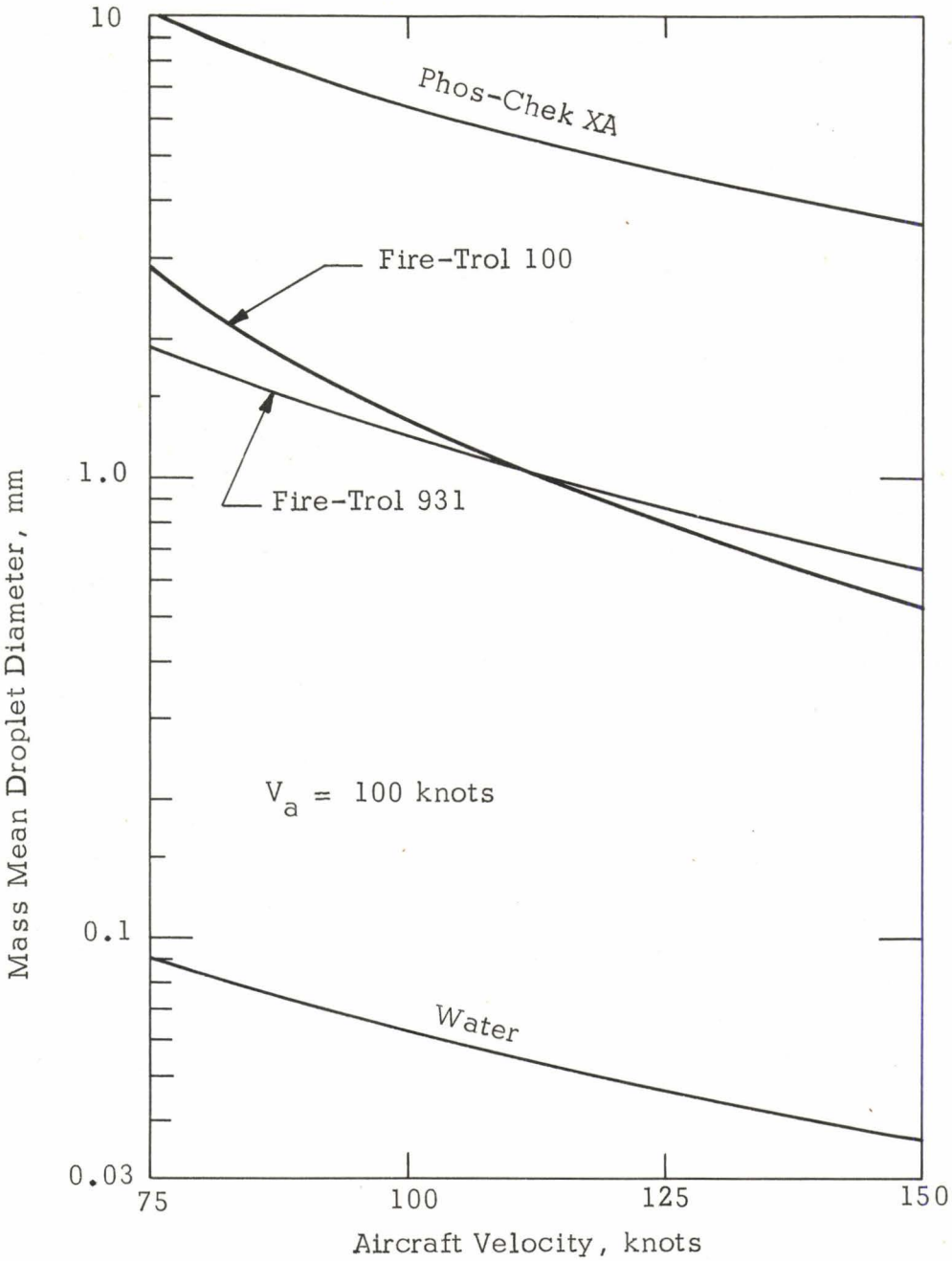

Figure 11. Computed Final Average Droplet Sizes in the Effective Ground Pattern.

An examination of the preceding table and figure shows that the mean droplet size decreases with increase in aircraft velocity, and that the droplet size of Phos-Chek is roughly a hundred times larger than that of water, and five times larger than that of the Fire-Trol solutions. The particle size of the two Fire-Trol solutions is roughly the same, with the computed values of FT 100 being largest at the lower aircraft velocities and smallest at the higher velocities. This results from the crossing of their effective viscosity curves shown in Figure 6. The mean droplet sizes at 100 knots are 6.5, 1.3, 1.3 and 0.06 mm for Phos-Chek, FT 100, FT 931 and water, respectively, and these values are roughly double the values computed earlier[1] and for the initial peripheral stripping region (Section 3.1). This results from the reduced liquid velocity brought about by air drag during the Taylor breakup process.

3.2.4 Droplet Size Distribution

An estimate of the terminal size distribution of the droplets falling in the effective ground coverage region is shown in Figure 12. The distribution is assumed to be given by the log normal probability distribution function, as discussed earlier. The mean value is that computed using the Mayer equation. At the present time little information is available regarding the droplet sizes produced by the aerial dissemination of a liquid retardant. However the results for Phos-Chek are consistent with the Honeywell statement[2] that "cloud terminal velocities estimated from films suggest Phos-Chek droplets on the order of 0.5 to 1 cm in the final region of the trajectory." A preliminary exploratory camera study by the Aerospace Corporation[3] also suggests droplet sizes of this order, with a small fraction of even larger size.

3.2.5 Additional Considerations

The breakup of the liquid retardant by Taylor instability produces particles with a variety of sizes, and estimates of the mean size produced under various conditions were given in ref. 1. The initial horizontal velocity of these particles is significantly less than the aircraft velocity ($V \simeq 0.69\ V_a$), but is still sufficiently large that further breakup of many of the particles will occur during their fall. The breakup will occur predominantly by surface erosion, but some breakup by bag formation may also occur. For the velocity range under consideration, liquid drops normally undergo breakup predominantly by surface erosion except under conditions near the breakup limit (e.g., low velocity) when bag formation may occur. The time to breakup a particle by surface erosion and bag formation is given by Eq. (5) and Eq. (3), respectively, of ref. 1. Application of these equations show that the breakup is a relatively rapid event under most conditions, requiring a time period of only about several millisec or less except for relatively large particles. Thus most of the particles do not travel very far before they are broken up.

As individual particles undergo horizontal travel during free fall they slow down due to air drag. The deceleration is given by Eq. (10) and (11) (with $m = \rho_l(\pi d^3/6)$, where d is droplet diameter), which shows that large particles decelerate slowly, whereas very small particles are brought to rest very quickly. The breakup of the particle occurs concurrent with its decelerated travel. Since the breakup is very rapid under conditions that it will occur,

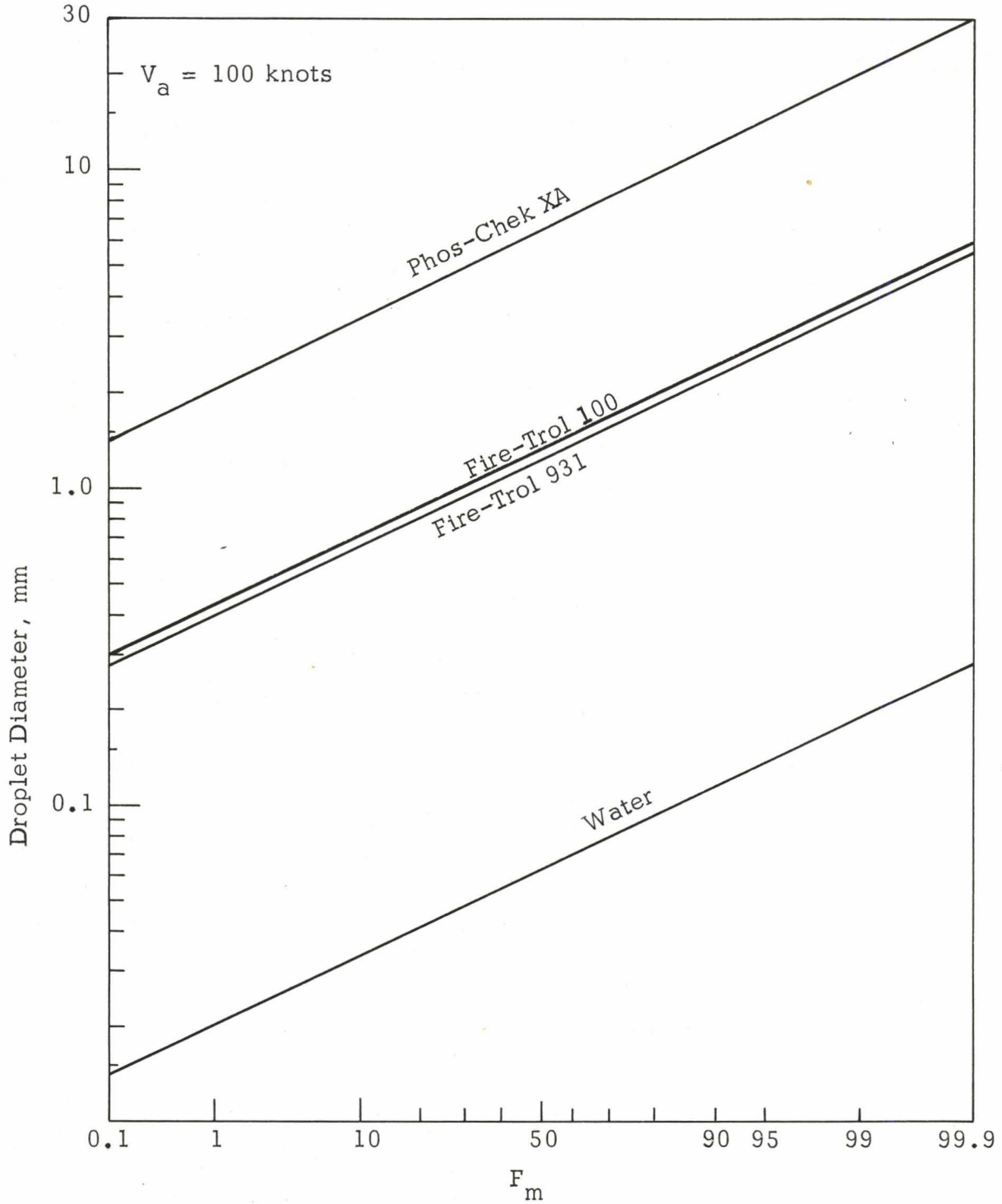

Figure 12. Computed Final Size Distribution of the Droplets in the Effective Ground Pattern. F_m is the Cumulative Percentage of Liquid Mass.

only the larger particles will travel any distance before they are broken up. The velocity vector of the droplets eroding from a moving particle is opposite to that of the particle motion, and hence the droplets produced by the breakup of a particle possess little forward velocity and in the absence of wind their trajectory is essentially straight downward.

As individual particles undergo horizontal travel and breakup, the core of any moving particle decelerates. A velocity is eventually reached which is no longer capable of causing further breakup of the particle by either surface stripping or bag formation. For ordinary low viscosity liquids the stabilizing force is surface tension, and the relation between particle diameter and the minimum particle velocity that will just not allow particle breakup is given by Eq. (1) of ref. 1. Application of this equation shows that breakup will not occur at velocities less than about 25 to 90 ft/sec for particles with diameters of 1 to 0.1 cm and surface tensions of 70 to 90 dyne/cm, respectively. These values are approximate and depend on the value of the drag coefficient. The liquid viscosity may also have some influence on the minimum velocity at which breakup will occur.

3.2.5.1 Effect of Fluid Elasticity

When the liquid is elastic, the elasticity confers an additional stabilizing force on the moving particle. In this case the preceding equation can be expressed approximately by

$$\frac{C_d \rho V^2}{2} = \frac{4\sigma}{d} + P_n \qquad (15)$$

where ρ is air density, V is particle (wind) velocity, σ,d are surface tension and particle diameter, and P_n is the normal elastic stress of the deforming liquid. From Eq. (30) of ref. 1, $P_n = \eta_s \dot{S}$. Application of this equation to Phos-Chek - whose surface tension is relatively low - indicates that the elastic stress increases significantly the air velocity required to breakup a drop of the liquid. It is consistent with the shock tube experiments conducted previously[1] that an air velocity of about 90 ft/sec will not breakup a 3-5 mm drop of Phos-Chek.

The preceding results indicate that the size of the liquid core remaining after particle breakup and deceleration to a stabilizing velocity is larger for an elastic liquid than for a nonelastic one. These particles consequently travel further before deceleration to terminal velocity than do particles of a nonelastic liquid. This together with the fact that the breakup rate of particles with high effective viscosity, η_e, is less than that with lower η_e indicates that the ground coverage path length will be longer for liquids with high η_e than for liquids with lower η_e.

3.2.5.2 Bag Breakup

Near the minimum air velocity necessary to breakup a liquid drop with a specified size, the breakup mechanism often involves the formation of a bag, followed by bag breakup which produces many small droplets. However the general behavior of the bag to shatter or breakup and produce many droplets - which is observed for nonelastic liquids - does not appear to be the same for highly elastic liquids such as Phos-Chek. In this case the bag merely appears to rupture and deflate without breaking up the drop, followed again by bag formation and deflation. An example of this behavior for Phos-Chek which was obtained in the shock tube studies is shown in Figure 13. This behavior again demonstrates the stabilizing effect that elasticity can confer on a liquid.

3.2.5.3 Effect of Viscosity on Droplet Size

The surface erosion model used to estimate terminal droplet size (i.e., the Mayer model) has been demonstrated to give reasonably good results for small drops and jets of Newtonian liquids subject to high wind flow. Its general validity for fire retardants - which are non-Newtonian and in some cases elastic fluids - breaking under relatively low wind flow conditions is not known, although it is believed that the model is applicable since it has been modified to include these fluid property effects. It should be pointed out however that most of the limited experimental studies of liquid breakup reported in the literature for small drops and jets indicate a viscosity power dependence, η^n, on resultant droplet size that varies between about 0.33-0.55. For example the carefully controlled studies of Weiss and Worsham showed[1] a viscosity dependence of n = 0.34; while the data correlation of Nukiyama and Tanasawa gave a mean value of 0.45. However the Mayer equation predicts a value of two-thirds (0.667), unless the parameter B - whose value is usually considered to be a constant - varies inversely with some power of the viscosity. If the true power dependence of viscosity is less than 0.67, there would be less difference between the calculated terminal droplet diameters of the various retardants than given in this report. The difference in the estimated droplet size effects (to be discussed subsequently) such as droplet settling time and wind drift would also be smaller. It may be mentioned that the Mayer model was used in the studies both because of its general success in describing liquid breakup, and because it provided a basis for estimating shear rate effect on the effective viscosity which is necessary in computing droplet size. No other model exists which allows this. However, if it were to be ultimately found experimentally in field testing that the viscosity power is significantly less than 0.67, then the Mayer equation could be modified empirically by means of the parameter B to include the true power dependence.

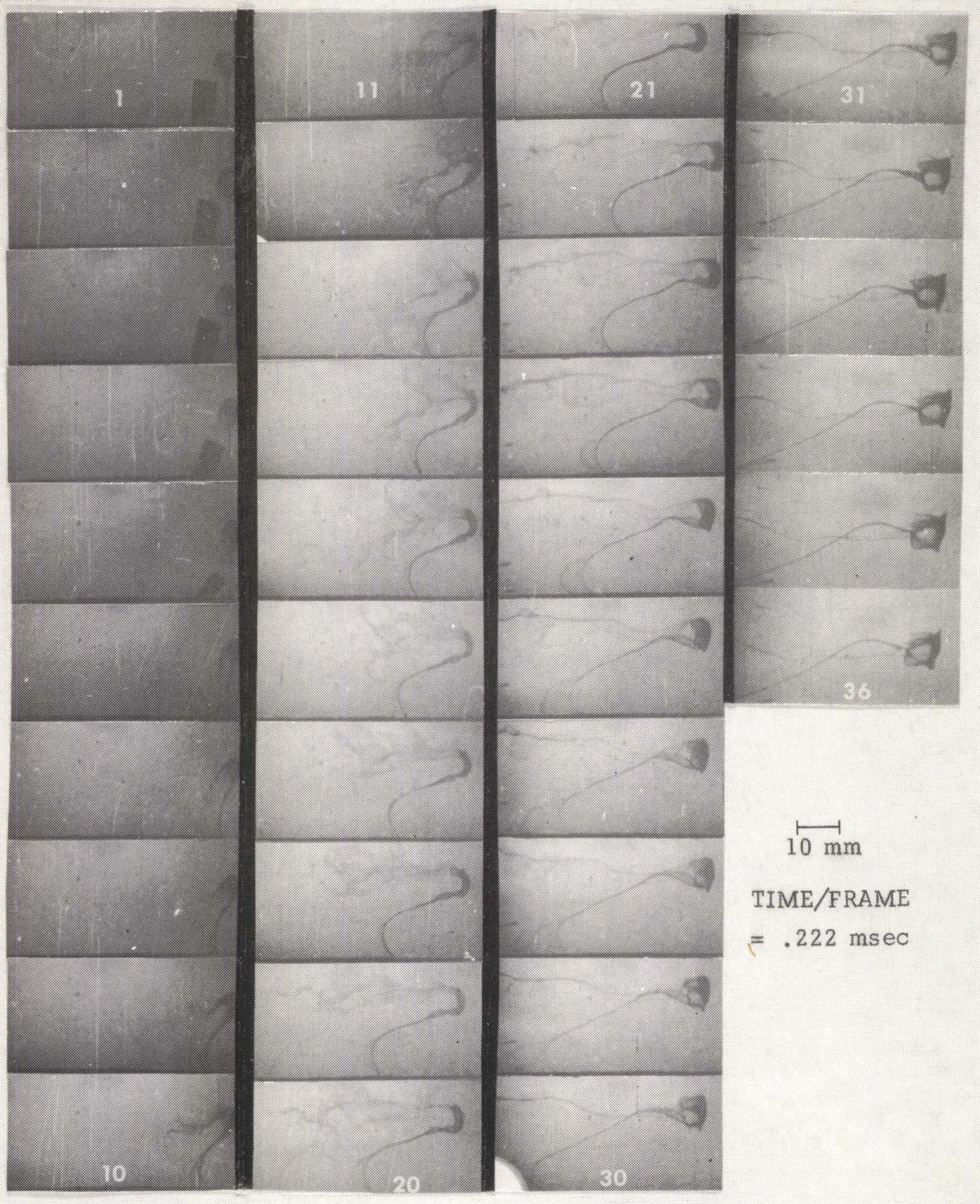

Figure 13. Photographic Sequence of the Aerodynamic Breakup Behavior of a Drop (5.7 mm) of Phos-Chek XA at a Wind Velocity of 90 ft/sec.

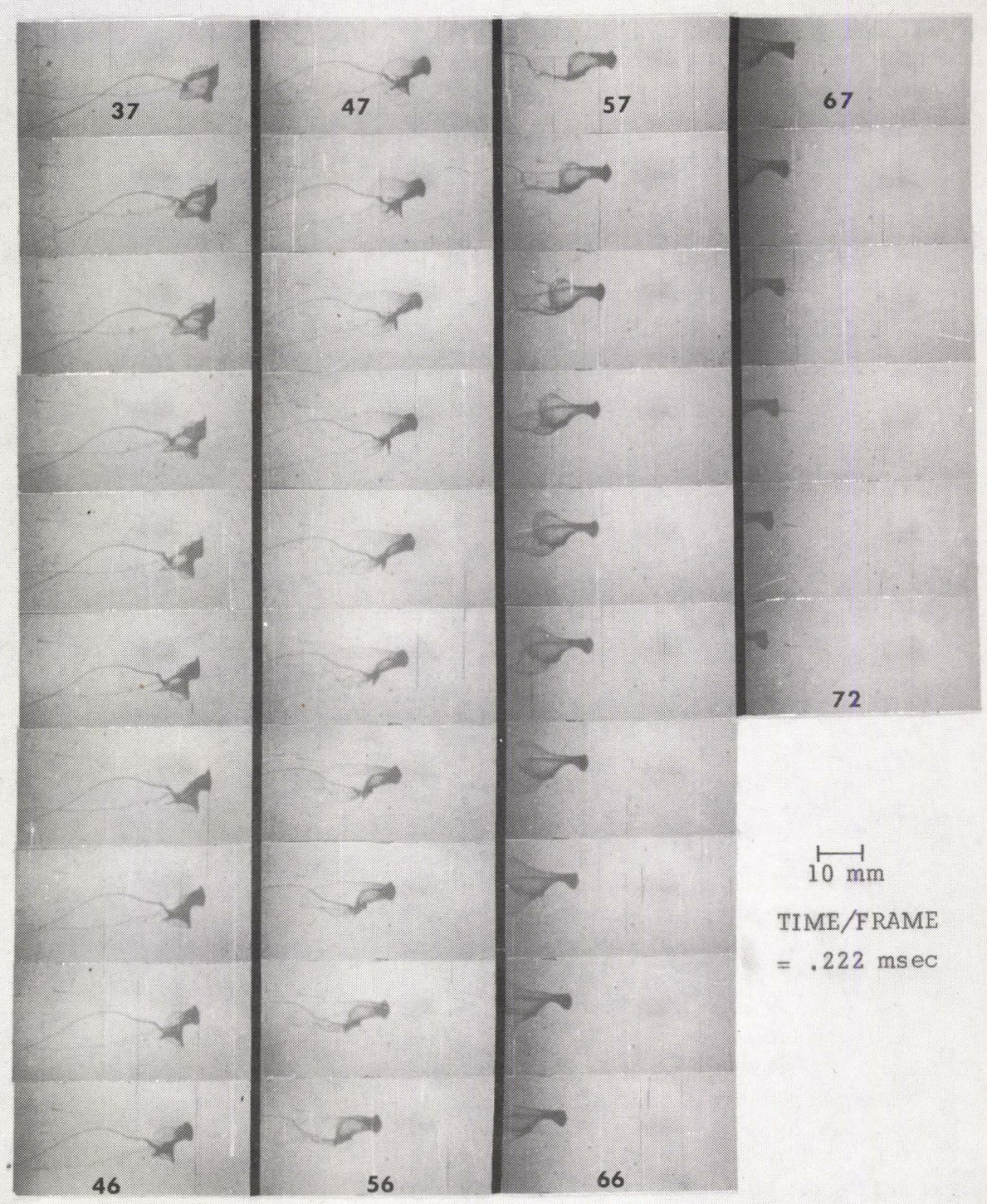

Figure 13. (Concluded)

3.3 DROPLET SETTLING

After their formation by ultimate breakup of the bulk liquid, the liquid droplets undergo settling. Depending on various conditions, many or all of the droplets reach their terminal velocity, V_t, by the time they reach the ground. Some of the droplets may have a forward or sideward component to their downward trajectory, which will affect the ground pattern of the disseminated liquid.

The terminal droplet velocity is given by Eq. (85) of ref. 1. Table IV summarizes these velocities for the mean particle size produced in both the initial peripheral stripping region and the effective ground pattern, assuming $C_d = 0.7$.

TABLE IV. ESTIMATED TERMINAL DROPLET VELOCITY (V_a = 100 knots).

Retardant	Initial Region		Effective Ground Pattern	
	d_m (mm)	V_t (ft/sec)	d_m	V_t
Phos-Chek XA	3.0	23.4	6.45	34.4
FT 100	0.9	12.8	1.33	15.5
FT 931	0.9	12.8	1.25	15.1
Water	0.042	2.8	0.063	3.4

The droplets produced initially in the drop fall more slowly than those that fall on the effective ground pattern, since they are smaller. The estimated terminal velocity of Phos-Chek is about double that of the Fire-Trol liquids, and an order of magnitude larger than that of water. Larger terminal velocities result in shorter airborne times of the falling droplets, and hence in less evaporation and wind drift of the droplets. Larger droplets also have less exposed surface area for evaporation per unit mass of liquid. The results of Table IV indicate that the evaporation loss of Phos-Chek during aerial dissemination should be significantly lower than for the other retardants, while water should suffer the greatest evaporation loss. The general ordering of the retardants for evaporation

loss indicated by the table is consistent with the findings of George[4,5]. The time required for the droplets to first reach the ground is greatest for water and least for Phos-Chek, and the cloud settling time is also in this order. Evaporation loss should increase with increase in aircraft velocity (smaller particles are formed), and increase in drop altitude (larger settling time). These conclusions are also consistent with experimental data.[4,5]

3.3.1 Wind Drift

The drift of the droplets by wind during their settling also depends on the particle size. Larger particles have larger inertia toward wind drift than smaller particles, and hence travel a shorter distance in a specified time period. The horizontal distance, z, traveled by a droplet with diameter d in time t when accelerated by an airstream with velocity, u, is given by

$$z = u\,t - (1/K)\,\ell n\,(Ku\,t + 1) \qquad (16)$$

where K is given by Eq. (11) with $m = \rho_1 (\pi d^3/6)$. The estimated drift in the effective region of the mean size droplets of Phos-Chek, Fire-Trol 100 and 931, and water in a 5 knot wind in 5 sec is about 15.2, 29 and 40.8 ft, respectively; while in a 15 knot wind the drift is 76, 107 and 125 ft. However the relative drift during the settling of the various retardants may be greater than these numbers indicate since the terminal velocities - and hence settling times - of the retardants are not equal. Table V shows the computed drift of the mean sized particles of the retardants settling from 200 and 100 ft altitude while subjected to a wind flow of 5 and 15 knots. The data given in Table IV was used in these calculations, and the value of the drag coefficient was assumed to be 0.7.

TABLE V. ESTIMATED WIND DRIFT OF THE SETTLING DROPLETS.*

Retardant	Settling Altitude (ft)	Settling Time (sec)	Wind Velocity (knots)	Droplet Drift (ft)	Wind Velocity (knots)	Droplet Drift (ft)
Phos-Chek XA	200	5.8	5	17.7	15	88
Fire-Trol 100 & 931	200	13.1	5	89.8	15	303
Water	200	59	5	497	15	1490
PC	100	2.9	5	5.6	15	32.9
FT 100 & 931	100	6.5	5	39	15	142
Water	100	30	5	251	15	757

*Neglecting Evaporation

It will be observed from the table that the computed wind drift of Phos-Chek droplets during settling is significantly smaller than that of water, while the value of the Fire-Trol solutions lies in-between. The drift of the droplets depends strongly on both wind velocity and settling altitude. The values given in the table are for the mean sized droplets, but there may be droplet size distribution effects on the wind drift of a settling droplet cloud. According to the single particle drag model used in the computations, the small droplets in a particle cloud should drift faster than the larger droplets, which may cause a partial separation of the particle sizes and - depending on wind direction - a general broadening of the cloud. However there is evidence that the effects of particle separation and cloud broadening are generally small, and that the major effect of wind drift is to move the particle cloud as a whole windward from the expected aimpoint.[2] The reason given is that small droplets in the cloud become entrained in the wakes of larger drops, and consequently have essentially the same fall velocity and settling time. On the other hand the relatively large experimental differences sometimes found in the ground pattern area containing very low retardant concentration (< 0.2 gal/C) under essentially the same dissemination conditions,[4,6] would appear to imply that droplet separation and/or cloud broadening may occur under appropriate conditions.

The preceding calculations indicate that there should be significant differences in the behavior (e.g., wind drift) of the settling droplets of Phos-Chek, the Fire-Trols and water. These differences arise through the differences in their calculated mean droplet sizes (Table III) - which result from differences in the effective viscosity of the fluids. However field test data appear to indicate that the differences in behavior of the droplets of water and the Fire-Trol solutions are much smaller than the preceding calculations would indicate, and there are several possible reasons for this. In the first place it should be pointed out that the preceding simplified calculations of particle size effects (e.g., wind drift) are largely illustrative in nature, and are intended mainly to show trends and demonstrate how certain parameters - especially retardant rheology - can influence the settling properties of the dispersed droplets. More quantitatively accurate calculations would require more complex models and analysis regarding the history of the falling particles. For example it is not to be expected that the simple single particle drag model can accurately describe the wind drift of a cloud of particles. Likewise the estimates of particle settling time in Table V are based on the constant terminal velocities of the droplets given in Table IV, but the fall velocity history of the drops will in actuality be more complex and depend on the drop altitude.

Another reason that the difference in droplet behavior of water and the Fire-Trol solutions may be smaller than calculated is that the water droplets are very small and undergo significant evaporation under suitable conditions. The effective size of the water droplets that can undergo significant wind drift is therefore larger than the mean size used in the preceding calculations. This will reduce the estimated difference in the relative drift of water and the Fire-Trol solutions.

There is also the possibility that the differences in the terminal droplet size of the retardants may not be as large as calculated in Table III, as discussed in Section 3.2.5.3. This would be the case if the mean terminal droplet size depends on a lower power of viscosity than the value (2/3) that is contained in the Mayer model that was used to compute terminal droplet size.

For illustration purposes, Table VI shows the computed mean droplet sizes of the retardants assuming droplet size to depend on the one-third (1/3) power of effective viscosity as indicated by Eq. (8) of ref. 1, and normalizing the values to that of Phos-Chek in Table III.

TABLE VI. ESTIMATED PROPERTIES OF THE DROPLETS ASSUMING A ONE-THIRD POWER VISCOSITY DEPENDENCE ON DROPLET SIZE[1]

Retardant	Mean Diameter (mm)	Terminal Velocity (ft/sec)	Settling Time[2] (sec)	Wind Drift[3] (ft)
Phos-Chek XA	6.45	34.3	2.92	32.9
Fire-Trol 100 & 931	2.60	21.8	4.60	86.3
Water	0.58	10.3	9.74	232

[1]Mean Droplet Size Normalized to that of Phos-Chek

[2]For a Settling Altitude of 100 ft

[3]For a Wind Speed of 15 knots

This reduces the spread in droplet size of the various retardants by one order of magnitude, and also reduces the spread in the droplet size effects of the retardants. For example for a settling altitude of 100 ft and a wind velocity of 15 knots it reduces the difference in the computed wind drift of the droplets of water and the Fire-Trol solutions from 615 to 146 ft. The evaporation of small water particles would further reduce the difference.

3.4 GROUND CONTOUR PATTERN

In ref. 1 a brief discussion was presented of the effects of retardant rheology on ground contour pattern. Some additional comments are given here in order to further illustrate the effects of various system parameters and retardant rheology on ground pattern, since it is known experimentally that many factors and parameters control the ground contour pattern.[4-6]

3.4.1 Ground Path Length

During an aerial drop of retardant, as the tank door is opened the retardant begins to exit and is subject to wind stripping at its exposed surfaces. The particle size of the eroded droplets that are formed was estimated previously. The concentration of retardant reaching the ground at any point beneath the flight path depends among other things on the surface area of exposed liquid falling from the aircraft. Thus the ground concentration of liquid increases with downrange distance since liquid continually exits the tank throughout the

tank exit time, which increases the surface area available for erosion. A larger tank load results in larger ground concentration since more liquid is exposed to surface stripping at any specified time during the liquid exit from the tank. This results because of faster flow rate, larger tank dimensions, or multiple (usually two) doors on the tank being opened simultaneously. However, the ground concentration in approximately the initial one-third of the total path length is always very low.

As the liquid exits the tank it is subjected to deformation as well as surface stripping, as discussed previously. However the falling bulk liquid largely keeps up with the aircraft during this phase of the drop. Eventually however, an element of the earliest dropped deformed liquid undergoes rapid deceleration and Taylor instability growth - terminating in the breakup of the liquid. This breakup then spreads to the remainder of the falling liquid, which retains its initial velocity until Taylor instability growth begins. The Taylor breakup of the liquid thus extends over a time period essentially equal to the tank exit time. However the breakup is not necessarily consecutive or uniform in the cloud since the flow rate from the tank is nonuniform and hence the thickness of the deforming liquid in the cloud is also nonuniform. After liquid breakup by Taylor instability growth, many of the resultant particles may subsequently undergo further breakup by surface erosion and bag formation - which results in a large concentration of liquid in the form of droplets descending on the ground. The size of these droplets was discussed previously. However many of these particles initially have a forward component of velocity until slowed by air drag, which tends to further increase path length.

The preceding concepts will be briefly illustrated for the CL 215 aircraft dropping a 700 gal load at 100 knots air speed (169 ft/sec). The computed numbers are mainly for illustration purposes and are not expected or intended to be quantitatively accurate. Nevertheless most of the results are generally reasonable in view of the approximations involved.

The tank exit time of the CL 215 aircraft has been estimated to be 0.75 sec,[7] although Forest Service studies[5,6] have indicated the value to be about 1.89 sec. The former value will be used here since this value was used previously in determining the constants in the Taylor breakup model.[1] Thus from the time of the initial opening of the tank until liquid exit is complete the plane travels approximately 0.75 (169) = 127 ft. The ground concentration of retardant increases throughout this distance but is always small. Depending on retardant composition (surface erosion rate and droplet size) and drop altitude, very little ground concentration may be obtained in a significant initial fraction of this path length. The Taylor breakup time of Phos-Chek with respect to the time that half of the liquid exits the tank is 1.605 sec.[1]

The computed values for other retardants are slightly smaller (water is 1.575 sec). The first half of the liquid exits in about 0.52 sec according to the flow rate curve given in ref. 7. Thus the plane travels (0.52 + 1.605)(169) = 359 ft from the initial opening of the tank until the liquid begins to break by Taylor instability growth. The ground concentration of liquid increases continuously through this distance, but the concentration in the first 127 ft is especially low. Since a significant portion of the path prior to Taylor breakup does not contain an effective (sufficiently large) concentration of liquid - but nevertheless contains liquid extracted by peripheral wind stripping (surface erosion) from the load - a fast breakup system will help maximize the amount of liquid contained in the meaningful (Taylor breakup) ground pattern area, as emphasized previously.[2] That is to say, faster breakup of the liquid by Taylor instability growth after exit from the aircraft results in less initial liquid loss by peripheral wind stripping and hence more liquid remaining for dissemination in the Taylor breakup region. The ground concentration of liquid in the Taylor breakup region then depends largely on the flow rate of the liquid from the tank (for specified drop height) since the Taylor breakup occurs over a time period roughly equal to the time period required to empty the tank. Thus faster liquid flow rates (shorter tank exit times) result in higher ground concentrations of retardant since the liquid load (minus initial surface stripping losses) is broken up and disseminated over a shorter ground path (neglecting particle projection effects).

The Taylor instability breakup of the liquid occurs over a distance of about 0.75(169) = 127 ft, and in this distance the ground concentration is greatest. Table 5 of ref. 5 shows that the path length for a ground concentration of 4 gal/100 ft^2 (the maximum concentration) for Phos-Chek XA, Gelgard, Fire-Trol 100 and water varies between 77 and 120 ft for a low altitude drop, and these lengths may be roughly (but not identically) compared with the value of 127 ft. The correlation can be made more apparent by an inspection of Tables 40-43 of the same reference, which give predicted values of contour lengths by concentration class. The high concentration contour lengths at low drop altitudes are produced largely in the Taylor breakup path and hence the two path lengths should be roughly comparable. On the other hand the lowest concentration (0.2 gal/100 ft^2) contour length roughly defines the total path length of the liquid from its initial exit from the aircraft until its Taylor breakup is complete. The calculated path length of 359 + 127 = 486 ft can be compared with the predicted values in the tables of 392 to 440 ft.

During the Taylor breakup of the liquid a portion of the droplets have an initial forward component of velocity which is about, $V = 0.69\ V_a$, as discussed previously. However not all the droplets are moving, since those formed by surface erosion or bag breakup have a trajectory that is straight downward. The forward moving (projected) droplets tend to increase the total (low and high concentration) path length. It also increases the length of the overall effective concentration path at the expense of the peak (very high) concentrations in the path. The increased path length depends on the altitude at which the droplets attain terminal velocity (hence on drop height), on the particle size (hence on retardant rheology), and to a more limited extent on the speed of the aircraft.

The horizontal distance, x, that a droplet with diameter, d, and initial velocity, V, moves (is projected) in time t is given by

$$x = (1/K)\, \ell n(KVt + 1) \qquad (17)$$

where K is given by Eq. (11). The time it takes for the same droplet - which has a terminal velocity, V_t, - to fall a distance y is given by, $t = y/V_t$. The distance that the liquid falls from the aircraft before it begins Taylor breakup is approximately $S = 0.5\, gt_f^2 = 0.5(32.2)(2.125)^2 \simeq 73$ ft. The estimated path length, x, that a mean sized particle of retardant with initial horizontal velocity, $V = 0.69\, V_a$, and falling with terminal velocity, V_t, travels before ground impact is given in Table VII for various drop altitudes, assuming the average C_d, in Eq. (17) is 0.8.

TABLE VII. ESTIMATED HORIZONTAL PATH LENGTH OF TRAVELING FALLING DROPLETS.

Drop Altitude	Phos-Chek XA		Fire-Trol 100 & 931		Water	
	t	x	t	x	t	x
(ft)	(sec)	(ft)	(sec)	(ft)	(sec)	(ft)
373	8.8	112	19.7	38	89	3.3
273	5.8	99	13.1	35	59	3.1
173	2.9	79	6.5	31	30	2.9
123	1.6	62	3.3	26	15	2.7

The values given in this table illustrate how particle travel after Taylor breakup extends the path length. Thus according to this table the total (low/high concentration) path length of Phos-Chek will increase about 50 ft when drop altitude is increased from 100 to 400 ft, and this is in agreement with Table 40 of ref. 5. On the other hand the path length of water will remain about the same - which is in rough agreement with Table 43. Tables 40-43 suggest that the effective path length ($C \geq 2$ gal/100 ft^2) at low altitudes is given roughly by the sum of half of the path length from the time of complete tank exit until Taylor breakup begins, the Taylor breakup path, and the droplet projection distance, i.e., by $0.5(359-127) + 127 + x$.

The preceding conclusion that the effective path length increases with increase in droplet size of the retardant (hence with its effective viscosity) is consistent with experimental studies which have shown that Phos-Chek produces larger effective pattern paths than Fire-Trol 100 and water.[4,5] An increase in aircraft velocity should therefore decrease the very high concentration path length (smaller particles are produced), and this has also been

observed experimentally.[5] The path lengths illustrated in Table VI are based on mean droplet size, and the effect of particle size distribution will further alter the path length and concentration. Changes in drag coefficient can also produce significant changes in calculated path length.

3.4.2 Ground Path Width and Area

Experimental studies have shown that during the aerial dissemination of a liquid retardant, the liquid undergoes lateral spreading, which results in a ground path that is much wider than the tank.[4,5] In general the total path width increases with increase in drop height, although this effect is often masked to some extent by liquid evaporation and wind drift. Increasing drop height tends to increase the average concentration of liquid near the sides of the path at the expense of the larger concentrations in the middle of the path, i.e., it reduces concentration peaking.

As discussed in ref. 1, the wind deformation of the bulk liquid prior to its breakup by Taylor instability increases the lateral extension of the liquid (given by R_e/R_o of the Taylor breakup model), and imparts a lateral velocity to the liquid. The maximum initial velocity on the outer periphery of the deformed liquid before Taylor breakup is V_e. The computed value of R_e for the various retardants is about 32 ft, and this value should roughly define the width of the high concentration ground pattern at low drop heights. Tables 35, 38, 40 and 43 of ref. 5 show that the path width is about 34 ft for a ground concentration of $C \geq 2$ gal/100 ft^2 for both Phos-Chek and water at 100 ft drop height. At larger drop heights the high concentration path widths become more narrow and the lower concentration path widths broaden. The effect appears to be more pronounced for water than for Phos-Chek, suggesting that its lateral spreading is faster. This agrees with statements by workers in the field that the ground paths are more compact for Phos-Chek than for water - which implies less lateral spreading ability for Phos-Chek than for water. However there is some question regarding the actual relative spreading characteristics of the retardants since the composition and altitude effects are obscured to some degree by liquid evaporation, path lengthening and wind drift.

In ref. 1 it was assumed that the lateral velocity, V_e, imparted to the liquid during its wind deformation serves as a driving force to increase path width with increase in altitude. The path width then increases with increase in particle size and drop altitude. On this basis the path width can be estimated using Eq. (17) and the values of terminal velocity and R_e/R_o. The resulting estimated path widths (including R_e) for drop heights of 373, 273, 173 and 123 ft for Phos-Chek are 167, 145, 110 and 87 ft. The corresponding values for Fire-Trol 100 and 931 are 89, 84, 75 and 66 ft, while for water they are 38, 37, 37 and 37 ft, respectively. These values indicate that the total path width

of Phos-Chek is much greater than that of the Fire-Trol retardants and water, due to its larger particle size. This appears contrary to the experimental evidence, although there is some question regarding the actual total path widths of the various retardants.

It is possible that during the Taylor breakup of the liquid that the lateral velocity produced by deformation is greatly reduced. On the other hand conservation conditions indicate that the Taylor breakup itself should impart a lateral velocity to the liquid. The radial velocity, V_r, in this case is given approximately by

$$V_r \simeq \frac{v_i R_e}{2 L_e} = \frac{R_e}{2 t_i} \qquad (18)$$

where v_i is the average velocity of the growth of the Taylor instabilities, L_e is the liquid thickness at Taylor breakup and t_i is the time required for the instabilities to breakup the deformed liquid (Eq. 12). Evaluating Eq. (18) indicates that the value of V_r is essentially the same as V_e. The present treatment thus suggests that the deformation and Taylor breakup should impart a lateral velocity to the liquid, and that the ultimate projection distance determining path width should increase with drop height and retardant droplet size. However the present experimental data seems to indicate that path width is essentially independent of droplet size, or may even decrease with droplet size.

In addition to path spreading by lateral droplet projection, the settling cloud may also spread by diffusion, and involve such factors as wind conditions, drop height and downwash of the aircraft. The general mechanism of the diffusion process is not understood, but for illustration purposes it may be assumed to roughly obey the Einstein diffusion equation, i.e.,

$$L^2 = 2 D t \qquad (19)$$

where L^2 is the mean square lateral displacement of a settling particle at time t, and D is the diffusion coefficient. The value of t can be identified with the settling time, and hence the lateral particle displacement will increase with increase in drop height. The value of D may depend on a variety of factors including droplet size. It should increase with decrease in droplet size since smaller particles can undergo random displacement more easily than larger particles. Thus lateral particle drift and hence path width should increase with decrease in droplet size by this mechanism.

It is possible that both of the preceding mechanisms, i.e., lateral particle projection and diffusion, occur simultaneously during cloud settling which may reduce the overall effect of droplet size on path width during cloud settling. At the present time however, the overall mechanism that controls cloud spreading during settling is not understood, and there is some question regarding the differences that exist between various retardants.

4. RETARDANT IMPACTION AND FLOW ON FUELS

Various studies have shown that the wetting of a fuel by aerial delivered fire retardant involves the impaction and splattering of individual liquid drops on portions of the fuel, followed by run (i.e., flow) and drip of the liquid over other portions of the fuel. Thus drop impaction effects are of significant importance in the wetting-out process, but little is known regarding the impaction process. In studies conducted earlier,[1] single drops of retardant were dropped on fuel samples and the final spread area measured. It was found that clear differences in area coverage by different retardants could be distinguished, and that the rheological properties of the retardant can apparently have an effect on both the droplet impaction and subsequent liquid flow process.

In the current program the earlier studies were continued in order to further understand the impaction and flow of single drops of liquid fire retardant falling on a fuel surface. These studies included high speed photography of the impaction process - including the measurement of the final spread area (hence average liquid film thickness) of the various retardants, and the development of mathematical models that describe the flow process and liquid spread area in terms of the important parameters and factors that control them.

4.1 EXPERIMENTAL STUDIES

The experiments consisted of dropping individual drops of the retardant on either a white matte finish cardboard target with a 1/2" ruled grid, or a wood dowel length, and photographing the resultant spread of the liquid by high speed photography. A system of two mirrors was used which enabled both a top and side view of the target area. Most of the experiments were conducted from a drop height of 40 ft, but some experiments were conducted at a lower height (11.5 ft) to study the effect of impact velocity. In order to minimize the effects of wind drift, a 40 ft high scaffolding was erected to support a 6" I.D., 40 ft high galvanized metal tube through which the drops fell. This reduced the drift of the drops to several inches from the previous several feet. However, even a drift of a few inches could move a droplet out of the camera's field of view, and therefore a plastic mask with an aperture 1" x 1/2" was fitted over the end of the tube to pass only those droplets that would land in the desired area. Using the aperture, approximately 8% of Fire-Trol 931 and water droplets generated would be admitted, Phos-Chek droplets would pass through about 5% of the time and Fire-Trol 100 only about 2% of the time. The more viscous liquid drops had higher lateral drift rates because they initially contained a tail.

Immediately below the aperture was a light extinction photo detector which sensed the presence of a droplet and initiated the flash sequence to photograph the event. The droplet target was located below the photo detector. The event was photographed with a Beckman and Whitley "DYNAFAX" high speed camera at a framing rate of 9600 fps. Every other frame was used for analysis, thus yielding an effective framing rate of 4800 fps. The total camera writing time was approximately 23 millisec at this speed; an electronic flash of 17.5 millisec duration provided the light and shuttering action for the photography.

Analysis of the recorded information was made from enlargements of the photographs. Fiducials in the field of view provided a constant reference in order to normalize the measurements that were made. The camera pictures provided a measure of the drop diameter and impact velocity as well as the liquid flow history. In addition however, calibrations were performed in the manner used previously[1] to determine drop size. Calculations using the drag equations for a falling drop (given in Appendix I) indicated that the impact velocities produced by the 40 ft drop height were within about 95-99% of the true terminal velocities.

4.1.1 Results of the Drop Spreading Experiments

The general behavior of the impact of drops of Phos-Chek XA, Fire-Trol 100, Fire-Trol 931 and water (colored with India ink) with a matte finish cardboard surface at roughly 31 ft/sec is shown by the selected frames of the photo sequences given in Figure 14. The impaction causes the liquid to undergo a rapid cylindrically diverging flow, which gradually slows down and finally stops. During the flow process, instabilities may develop on the front of the advancing liquid and grow with time. The growth of the instabilities is related to the viscous and elastic nature of the liquid. Instabilities do not develop on Phos-Chek which is both highly viscous and elastic, (has a high effective viscosity), and are not very pronounced on Fire-Trol 931 which is also elastic. They become well developed in water and Fire-Trol 100, which are non-elastic liquids. The instabilities generated on the cardboard surface are generally less pronounced than previously formed on the plywood surface - which were larger and more in the form of streamers.[1] The streamers may be due in part to the nature of the impact surface, and the presence of trapped air bubbles - as suggested in the Fire-Trol 100 photos.

A comparison of the rate of liquid spreading of the retardants by impaction is shown in Figure 15, where the spread factor is shown as a function of time. The spread factor is given by A/V, where A is the area of the spread liquid and V is the volume of the drop. The reciprocal of A/V defines the average film thickness of the spread liquid. It may be seen that both the rate of spread and the final value of the spread factor decreases with increase in the effective viscosity of the liquid. However the impact surface may also play a role since it was previously found that the spread factor of Fire-Trol 100 on plywood is a little smaller than that of Phos-Chek, whereas the opposite is true for the cardboard. In general there is rough but satisfactory agreement between the spread factors found on the cardboard surface and those found previously on the plywood surface. A part of the generally small differences between the two sets of results is that it was more difficult to measure the spread area accurately on the plywood surface, where more streamer formation occurred.

A further interesting observation from Figure 15 is that it may be seen that at about the time that the spreading liquid is brought to rest, the area of Phos-Chek and Fire-Trol 931 decreases slightly, whereas that of water and Fire-Trol 100 remain essentially constant. This is probably related to the elastic nature of the former two liquids.

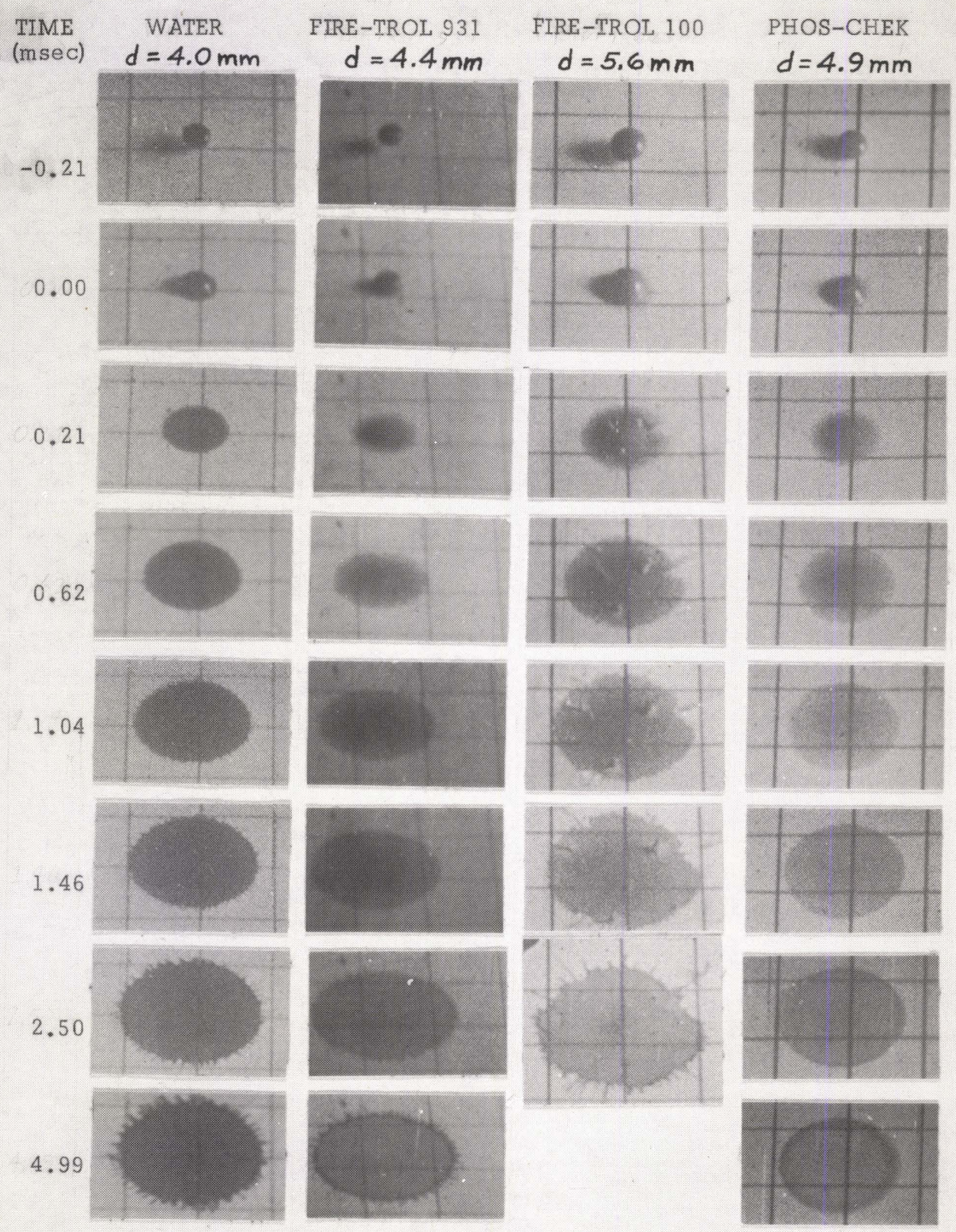

Figure 14. Selected Frames From Photographic Sequences of the Impaction of 4-6 mm Drops of Various Liquid Retardants With Cardboard. Average Impact Velocity is 31 ft/sec.

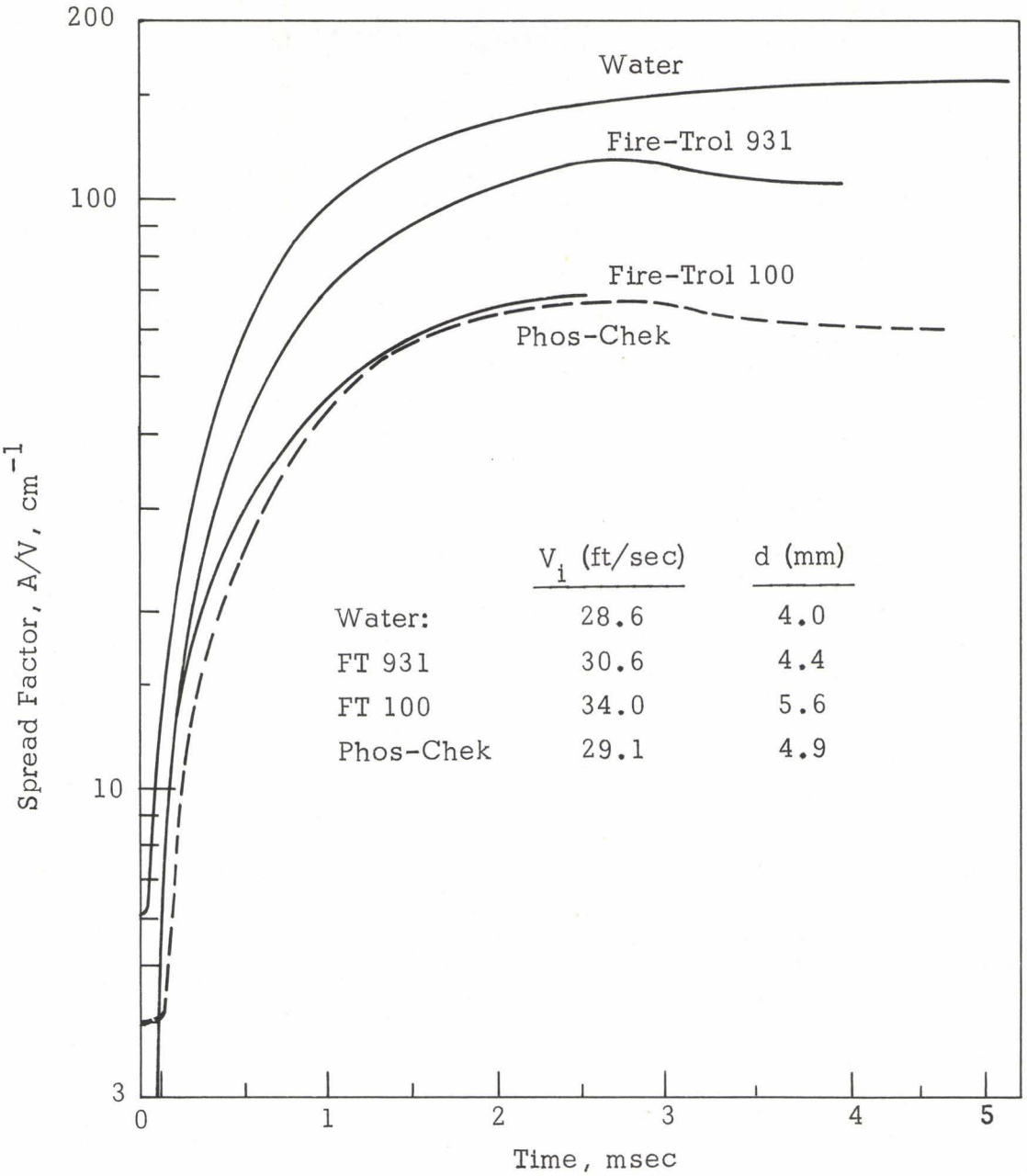

Figure 15. Comparison of the Spreading Behavior of Drops of the Retardants Impacting With a Cardboard Surface.

4.1.1.1 Effect of Impact Velocity and Drop Size

Experiments were also conducted to determine the effect of impact velocity and drop size on liquid spreading characteristics, and Figure 16 shows the results for Fire-Trol 100. Impact velocity was changed by dropping the drop at a lower drop height (11.5 ft). Reducing impact velocity reduces the rate of spread and the final spread factor. However the general effect is not especially pronounced. Reducing the velocity to 75% of the 40 ft fall value reduced the spread factor to 87% of the corresponding value, or about a 0.5% decrease in spread area for every 1% decrease in impact velocity.

Increasing the drop size also reduces the spread factor, and here the effect (for practical changes in the parameter) is larger. Increasing the drop size by a factor of 1.35 reduced the spread factor to about 0.7 of the 40 ft fall value, or about a 1 to 1 change. In this case the impact velocity was also about 20% higher.

4.1.2 Drop Impact with a Wood Dowel Length

Experiments were conducted to determine the nature of the impact process when a liquid drop interacts with a branch or twig. It had been previously conjectured that an elastic liquid like Phos-Chek may possibly wrap around the element. Figure 17 shows a Phos-Chek drop interacting with a 1/8" diam. wood dowel length. The photographs show the direct (face-on), top and side views of the event. It may be seen that the impact causes the liquid to spread and flow off of the element in the form of a sheet, which narrows down to a ligament near the end of the event. There is no evidence of wrap around during the impaction process.

Figure 18 shows a Fire-Trol 100 drop interacting with a 1/4" diam. wood dowel length. The flow process during the early stages in which a sheet is formed is the same as in Phos-Chek. However it differs in the latter stages in that the sheet maintains essentially its full width during the flow process, and then fractures along its entire length near the dowel. The behavior of the Phos-Chek sheet to narrow and form a ligament in the later stages is probably due to its elasticity.

4.2 ANALYTICAL STUDIES

In order to better understand the flow produced by drop impaction, and the parameters and factors that control both the rate of flow and the final liquid coverage area (spread factor), studies were conducted to develop models that will describe the flow process on a fundamental basis.

4.2.1 Static Spread of a Liquid Drop

When a liquid drop is placed on a non-absorbent surface it undergoes spreading by gravitational forces until the liquid film attains a final equilibrium state. It is envisioned that the final spread area is controlled by surface tension, and in order to help test this hypothesis, equations were developed

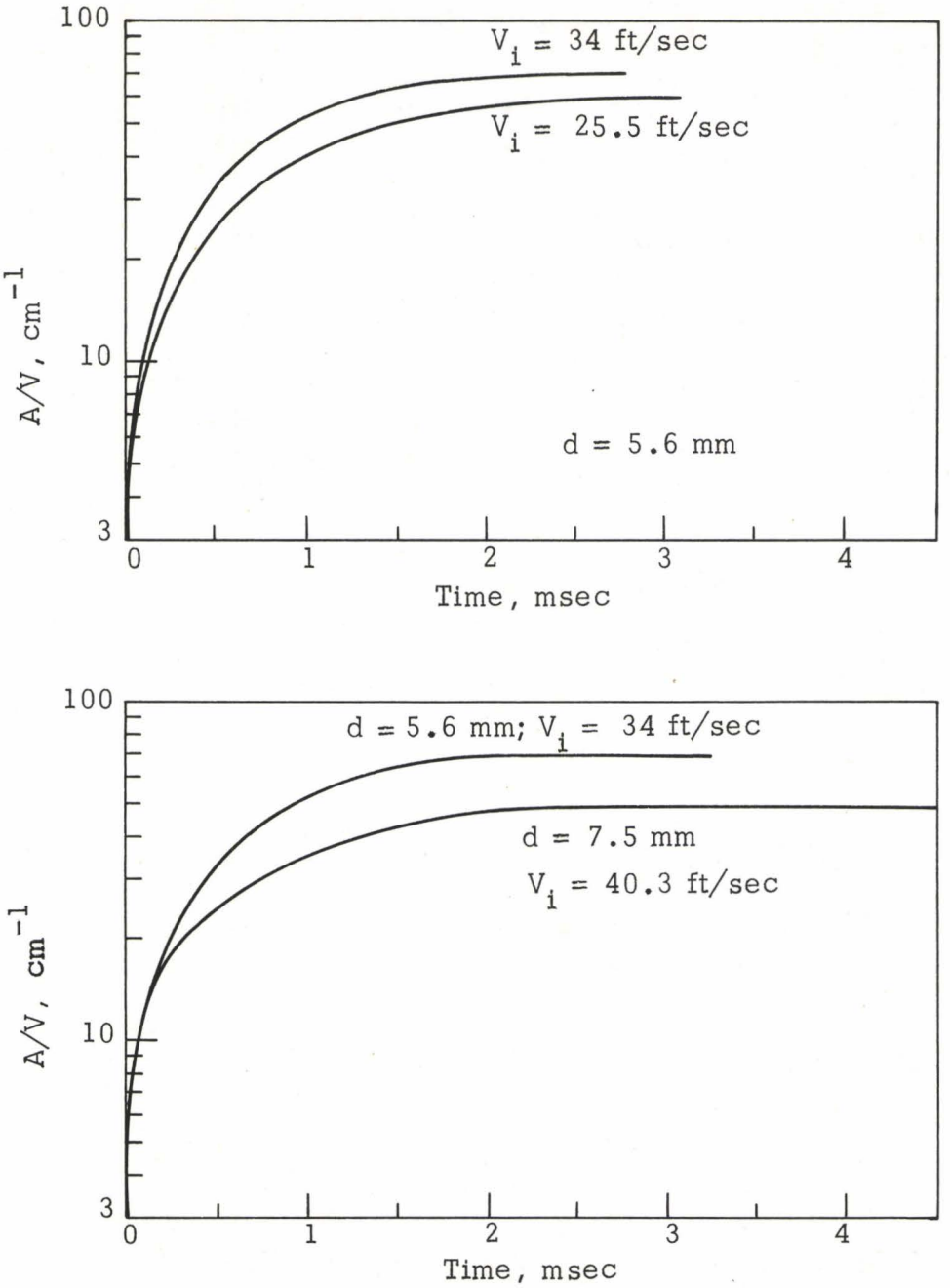

Figure 16. Effect of Impact Velocity and Drop Size on the Spreading Behavior of Fire-Trol 100.

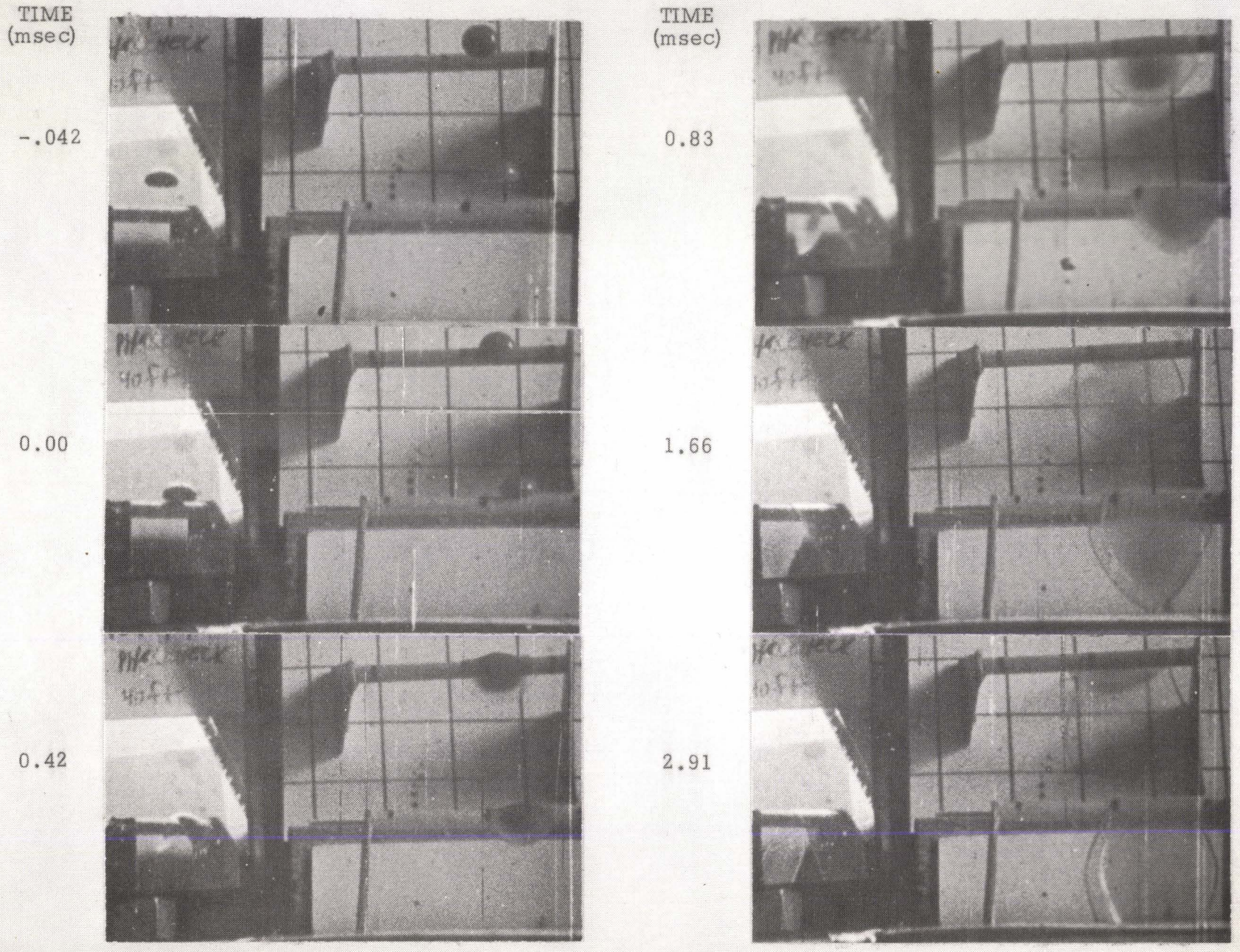

Figure 17. Selected Frames From the Impact of A Falling Drop (4.86 mm) of Phos-Chek With a 1/8" diam. Wood Dowel. V_i = 29.1 ft/sec.

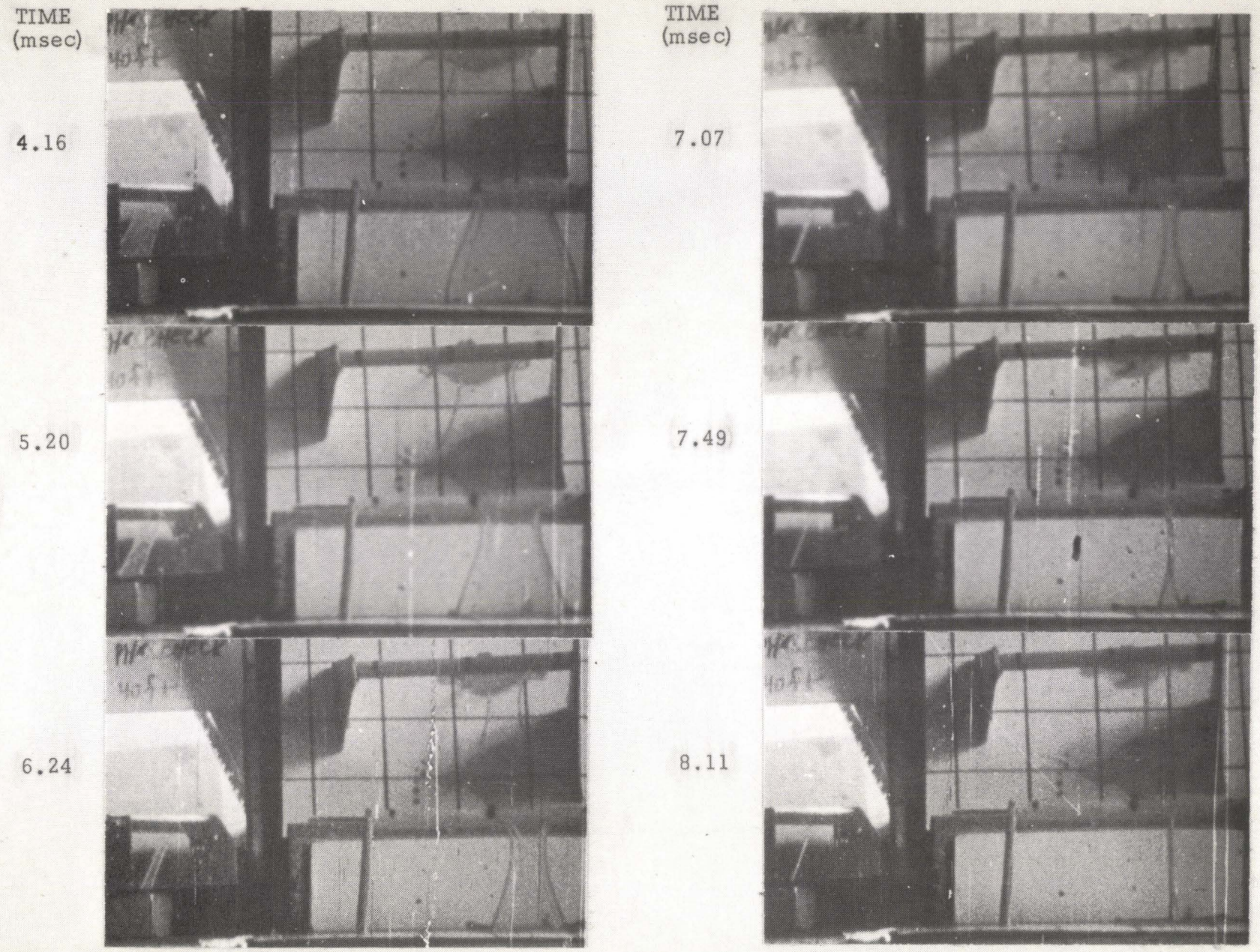

Figure 17. (Concluded)

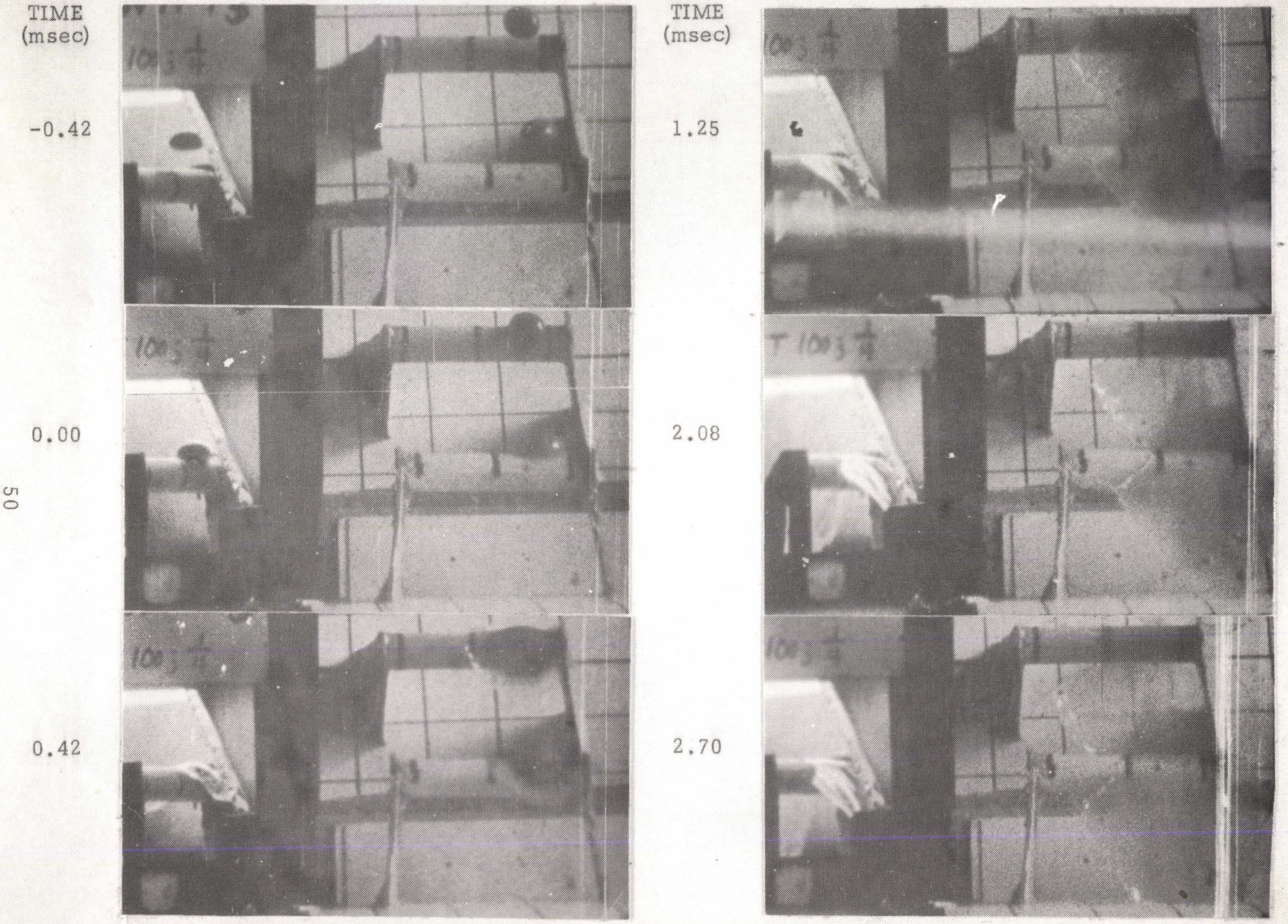

Figure 18. Selected Frames From the Impact of A Falling Drop (5.62 mm) of Fire-Trol 100 With a 1/4" diam. Wood Dowel. V_i = 34.3 ft/sec.

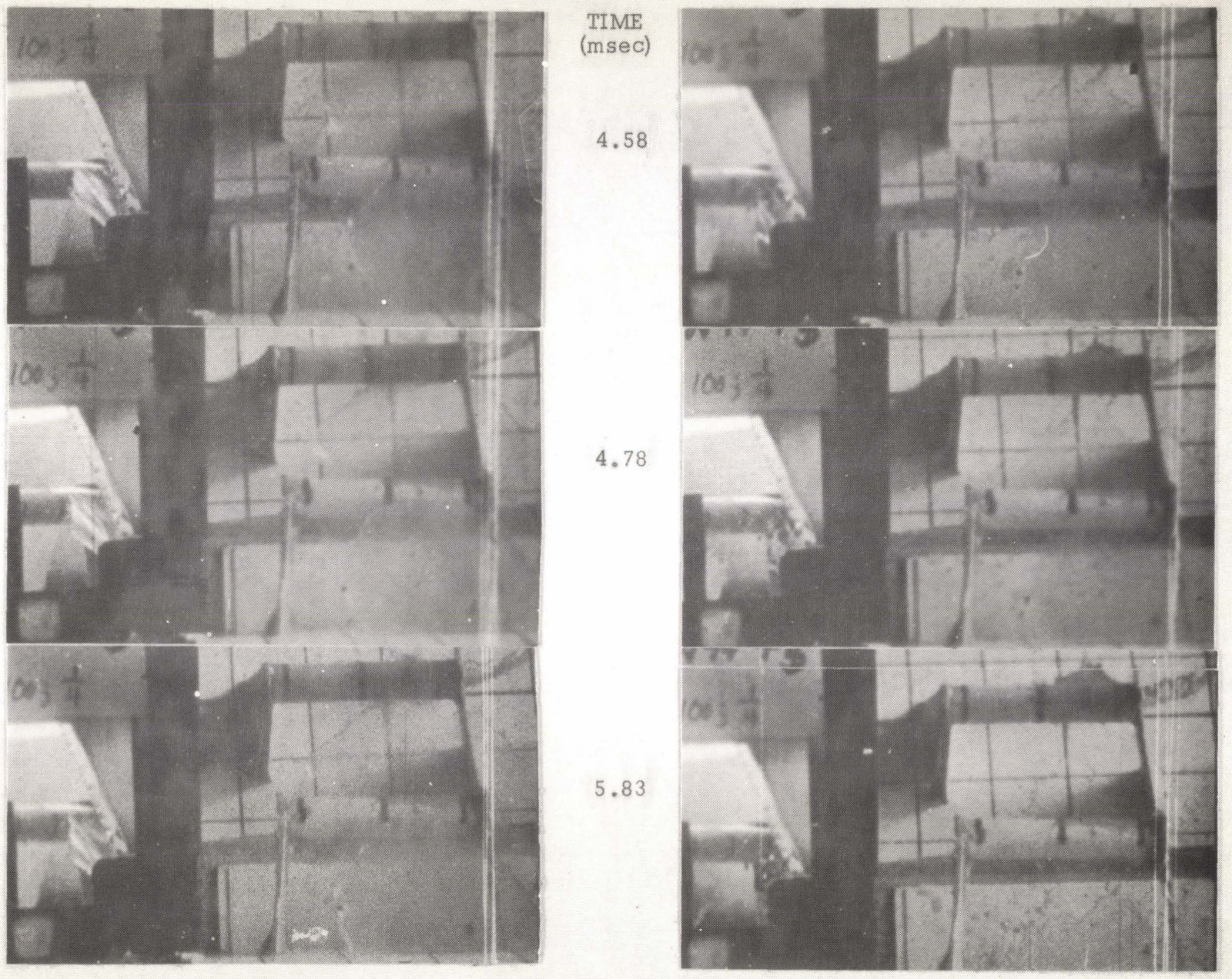

Figure 18. (Concluded)

that describe the equilibrium spread of a drop falling from a height onto a surface. These equations are given in Appendix II. For the case of the static spread of a drop, H is replaced by the drop radius, d/2, where d is drop diameter. The equations give the specific spread of the drop, i.e., A/V (called the spread factor) in terms of the contact angle, θ, between the solid surface and the outer edge of the liquid. Note that A/V - the ratio of the area of the spread liquid to drop volume - is the reciprocal of the average film thickness, h, of the spread liquid, i.e., $h = V/A$.

In practice the value of the contact angle is not usually known, but can be calculated using experimental values of the spread factor. Using average static values of A/V of 13, 5 and 11.1 for Phos-Chek, FT 100, and FT 931 obtained previously,[1] gives values of θ of about 90^{o}, 122^{o} and 89^{o}, respectively. These values are reasonable and imply that the contact angle of the outer edge of the liquid is essentially normal to the surface. The normalcy of the estimated values indicates that the assumption that surface tension essentially controls the static spread of a drop is probably quite good. The experimental spread factors actually varied slightly with material surface - indicating some absorption effects - but these changes do not alter the general magnitude of the computed values of the contact angle or the preceding general conclusions.

On the other hand when the experimental spread factors found for dynamic impact from the 40 ft drop height are used, the computed values of $\cos \theta$ vary from about -148 to -300. These values are nonsensical, and show that the liquid spread is not controlled by only surface tension in this case, but also involve other factors such as liquid kinetic energy and liquid viscosity.

4.2.2 Model of Dynamic Drop Spread Using An Assumed Flow Field

The spreading of a liquid drop brought on by impact has received only limited prior study. Engle photographed the spreading of a water drop impacting with a solid surface,[8] and found that the radial spread of liquid decreases rapidly with time and gradually stops. She found that the initial spreading velocity is greater than the impact velocity, and later studies have examined this finding in more detail analytically.[9] More recently the flow has been investigated in some detail numerically using a computer.[10] However liquid viscosity and surface tension were ignored in the calculations, due to the complexity of the problem.

In the present program studies were conducted to develop models that will describe the flow process on a fundamental basis in order to further understand the parameters and factors that control the spreading of a liquid drop impacting on a surface. The exact solution utilizing a two dimensional computer code containing liquid viscosity effects - which is available - was beyond the scope of the program in view of the cost and time involved. Instead analytical studies were conducted which attempted to understand the processes on a more physical basis.

The general approach toward the solution of the dynamic drop spreading problem pursued on the program was to assume the general form of the flow field produced by the impact, and then solve the problem on this basis subject to the real boundary conditions. In the initial studies a flow field essentially similar to that used previously for the deformation of a cylinder was assumed, and the problem then solved rigorously with all the constraints imposed by the conservation laws of fluid dynamics. This treatment contained the effects of both effective fluid viscosity and surface tension. It was found that although the model contained many features exhibited by the experimental data - particularly with regard to the effects of the controlling parameters - the time dependence of the flow differed significantly from that observed experimentally. Further studies suggested that it may be possible to modify the model to a satisfactory state, but in view of time limitations a less rigorous approach was adopted for the present purposes.

4.2.2 Model of Dynamic Drop Spread Based on Energy Conservation

The model ultimately developed to describe the liquid spreading produced by drop impact with a rigid surface is based on energy and mass conservation, without regard for momentum balance. Its derivation is given in Appendix III. This model was found to exhibit most of the important features of drop spreading observed experimentally, and is simple to use. In principle the model contains no unknown parameters. However in order to elucidate the average value of the viscosity that controls the liquid spread of the retardants, the equations were fit to the experimental data using a constant viscosity coefficient rather than the shear-rate dependent viscosity exhibited by the retardants. The results are shown in Figure 19. It may be seen that an excellent fit of the data is obtained. The viscosity giving these fits are 4 poise for both Phos-Chek and Fire-Trol 100, and 1.2 poise for Fire-Trol 931. The use of these viscosities then allows analytical estimates to be made of the drop spreading characteristics under other impact conditions that appear to be in relatively good agreement with experiment-based on the limited data available. Figure 20 illustrates the computed effect of drop size and impact velocity on the spread factors of the retardants.

Figure 21 shows parametric curves of the computed effect of impact velocity, drop size and liquid viscosity on spread factor. The spread factor increases almost linearly with increase in impact velocity, but the effect is not strong and is in rough agreement with experiment. It decreases with increase in drop size, and the effect is greater for smaller drops than for larger ones. Again the results are in rough agreement with experiment. The spread factor decreases with increase in fluid viscosity, but here the general effect appears to be much larger than that observed experimentally-particularly for water which has very low viscosity. The reason for this is not presently known.

Computations were also made to determine the effect of surface tension. It was found that the results are quite insensitive to the value of surface tension, which implies that surface tension has little effect on controlling dynamic droplet spread. This same conclusion is obtained by

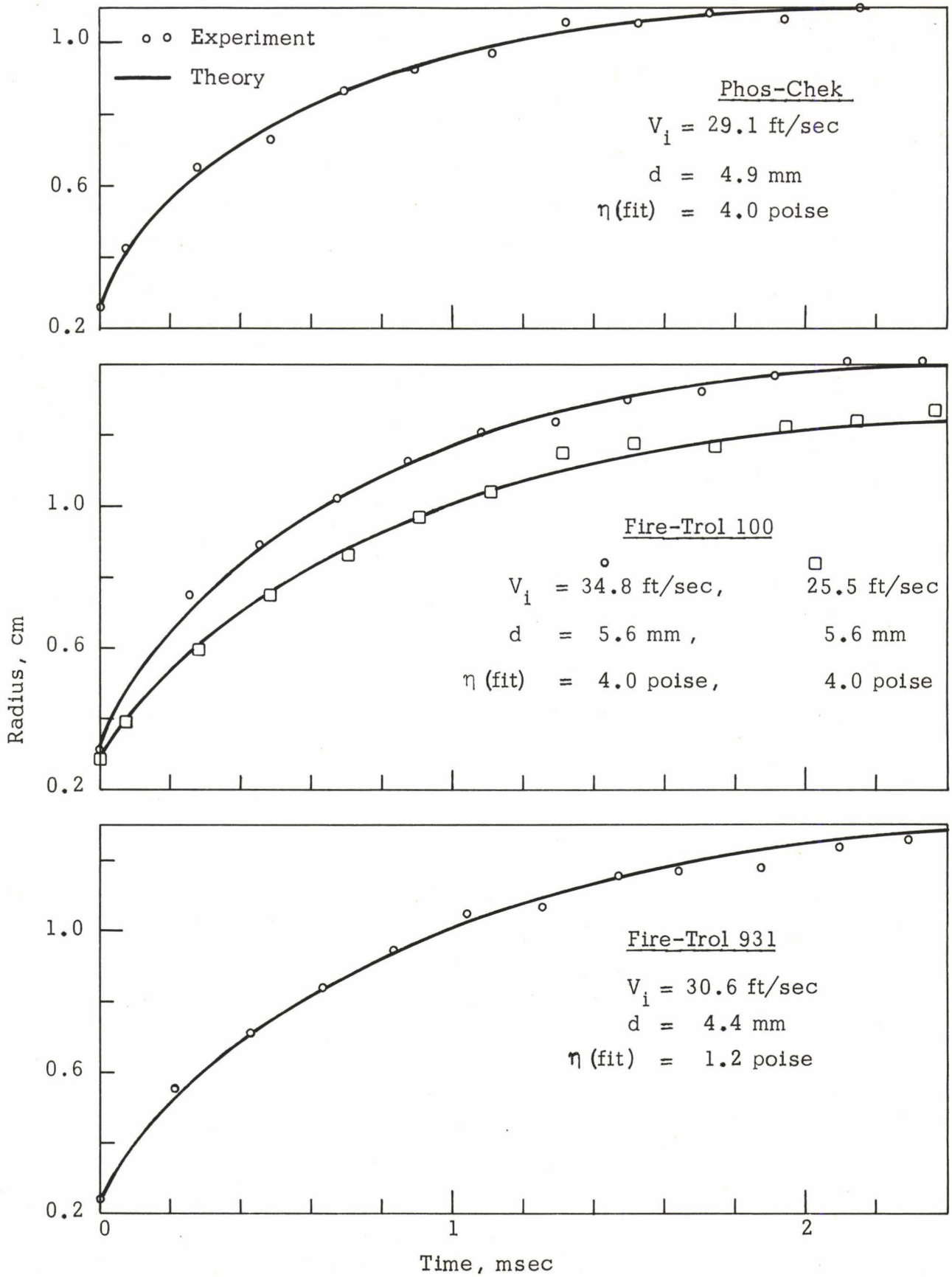

Figure 19. Comparison of Theoretical Liquid Spreading Rate With Experiment.

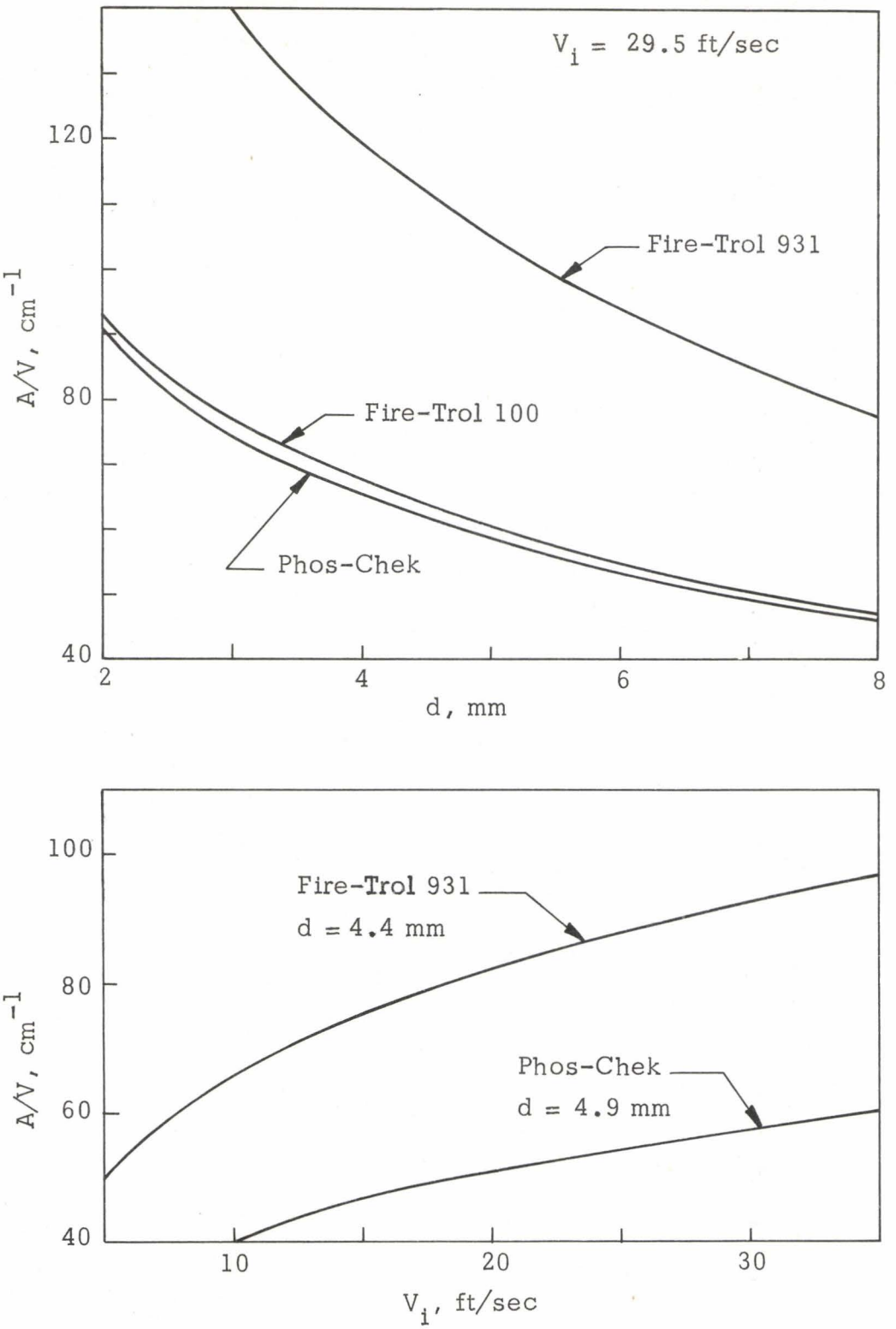

Figure 20. Theoretical Drop Spreading Curves for the Fire Retardants.

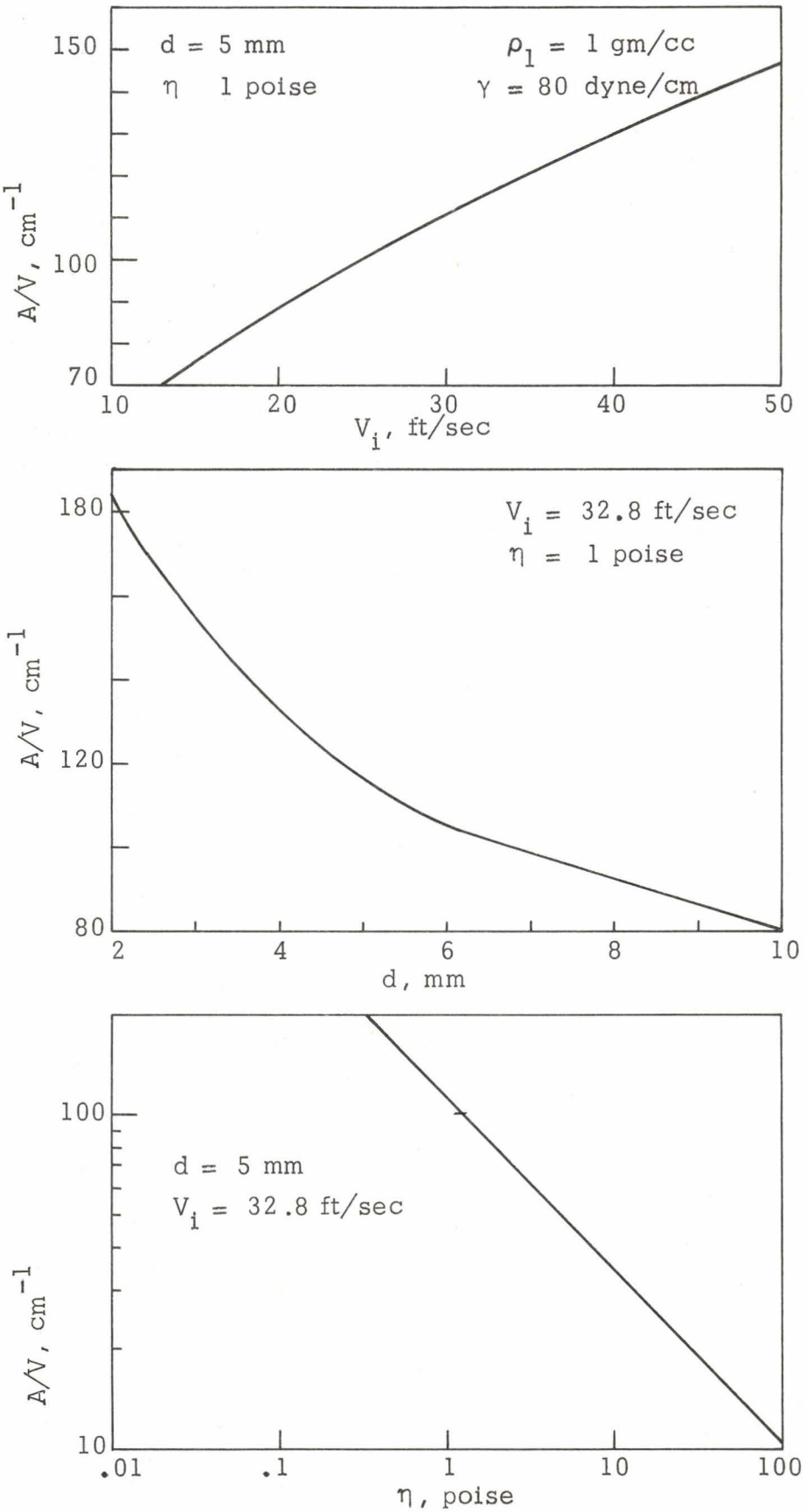

Figure 21. Theoretical Curves Showing Parameter Effects on Liquid Drop Spreading.

computing the surface energy of the spread liquid and comparing it with the kinetic energy of the falling drop. The only case where surface tension is of any significance is for the case of water where the estimated spread factors are very large. However these results are incompatible with experiment, as noted previously.

During drop spreading the shear rate of the liquid increases rapidly to some maximum value ($\sim 10^3$ sec^{-1}), and then decreases to zero. The viscosity of a non-Newtonian liquid varies throughout the flowing liquid both spacially and time-wise during the spreading process. It seems reasonable to believe that the flow can be described in terms of some average viscosity coefficient, and the application of the model to the experimental data confirms this belief. This viscosity then defines the average shear rate that determines the viscosity. The present studies indicates the values for Phos-Chek and Fire-Trol 100 are about 4 poise, and for Fire-Trol 931 is about 1.2 poise. These values are apparent viscosities, η_a, rather than effective viscosities, since the model is based only on energy conservation, and viscous energy dissipation results from the real viscosity component of the effective viscosity. Elastic energy is recoverable. Comparing the preceding values of viscosity with the real viscosity vs shear rate curve (Figure 23 of ref. 1) indicates the average controlling shear rate to be relatively low, i.e., 10-100 sec^{-1}.

5. CONCLUSIONS

On the present and preceding[1] program, analytical models were developed that describe the aerodynamic breakup of aerial delivered liquid fire retardant in terms of the important system parameters and fluid properties that control the dissemination process. Experimental measurements of fluid properties and aerodynamic breakup were also made to assist and provide data for the models. These models have provided a general understanding of the dissemination process in terms of the controlling factors, and allowed an estimate to be made of the terminal droplet size of various retardants under typical dissemination conditions. The droplet sizes have various implications regarding such things as liquid evaporation, wind drift and ground contour pattern.

The question arises regarding the general validity and applicability of the models, of which a number of comments may be made. In the first place it may be noted that the general purpose of a model is usually to provide a basis of understanding of a specified phenomenon in terms of the important factors and parameters that may control it. The important link in the understanding is that the model describes the fundamental processes which occur. In this case the model should be reasonably valid in describing qualitative trends and parameter effects, although the absolute values of the numbers predicted (apriori) may be only approximate or even completely wrong because of approximations made in the development of the theory, complex interactions which may occur between certain parameters under certain conditions, or significant gaps in the general understanding of various processes contained in the model.

With regard to the present models it is currently believed that these models are grounded on a sufficiently general basis that they will describe most of the gross effects of the system parameters and fluid properties on the dissemination process essentially correctly on at least a qualitative (and in some cases semiquantitative) basis. However, it will be recognized that some aspects of the models are highly simplified. For example, the treating of the beginning of the Taylor breakup process in terms of a breakup time involving the entire tank of retardant is a very rough approximation. This approximation however allows the effects of tank dimensions on the initial breakup characteristics of the liquid to be estimated, without consideration of the exact - but considerably more difficult problem - of estimating the deformation and Taylor breakup of the falling liquid whose downfall rate varies throughout the tank exit period. The approximation was compensated for by fitting the equations under several conditions by experimental breakup times determined by the Honeywell Corporation. The assumptions that the falling, deforming liquid has uniform thickness, and that the Taylor breakup process is uniform and produces only one size are also contrary to fact. However, they allow various conclusions regarding the effects of tank and gating system, aircraft velocity and fluid properties on liquid deceleration, breakup and dissemination. The estimated particle sizes at this stage of the overall breakup process are thus highly idealized, and probably represent some kind of a mean value of an actual distribution of sizes. The exact sizes are not of much consequence however since most of the particles undergo further breakup by surface erosion (at reduced velocity), and the estimate of terminal droplet size is made on this basis.

The surface erosion model used in these calculations, has been shown to give reasonably good results for small drops and jets of Newtonian liquids with relatively low viscosity, and it was modified on the current program[1] to include the effects of non-Newtonian viscosity and fluid elasticity. There is some question however, as to whether the Mayer model contains the correct dependence of the final droplet size on the fluid viscosity (if the parameter B is considered to be a constant) - as discussed earlier. Further information regarding this question can best be obtained by measuring the terminal droplet sizes produced in aerial dissemination tests with real retardant fluids, and comparing them with the predicted values. The theoretical model could then be modified empirically by means of the parameter B to include the observed viscosity dependence.

5.1 RETARDANT PROPERTIES DURING AERIAL DISSEMINATION

One of the most important conclusions resulting from the general program is that during the overall aerial dissemination of a liquid fire retardant, the liquid undergoes a variety of processes in which it is subjected to shearing at different rates. The rate of the shearing is controlled in part by various

system parameters such as aircraft velocity and the tank and gating system, and also by the effective viscosity of the liquid. However, the effective viscosity of the liquid is determined by the shear rate (for a non-Newtonian fluid), and thus for a given process a balance is established between the shear rate and viscosity. The functional relationship between effective viscosity and shear rate of a retardant is thus of some consequence on the aerial dissemination characteristics of the liquid.

On the program models were developed for estimating the shear rate of the various processes, and the solutions of the equations provided estimates of both the shear rate and effective viscosity. It is useful to summarize this data here, and Figure 22 shows the results. The initial deformation of the bulk liquid takes place under low shear rate conditions, and the magnitude of the effective viscosity for the non-Newtonian retardants is near their maximum values. However, viscosity has little effect on the deformation process, which is inertia controlled. The Taylor instability breakup occurs at a higher shear rate, which reduces the effective viscosity of the retardants. High viscosity retards the shear rate and can affect the Taylor breakup process. The surface erosion occurs at even larger shear rates, and consequently at lower effective viscosity. The table values are for the Taylor breakup (effective) region, and higher values are attained in the initial peripheral stripping of the liquid. The shear rate during droplet impaction decreases throughout the spreading process (to zero). The values given in the table are values that largely characterize the apparent viscosity required to describe the flow process.

5.2 RECOMMENDATIONS

On the basis of the results of the studies it is believed that the models developed can be used to provide useful information regarding potential changes that could be made in fire retardant composition (thickener concentration and type) for more effective or controlled dissemination of the retardant. For example, it may be found desirable in application to eventually vary the gum thickener concentration according to the specific drop conditions. Thus the optimum concentration of thickener may be different for low altitude drops on relatively flat country fires than for higher altitude drops on mountain fires or for night drop conditions. Alternatively there may be a near optimum concentration for general use that is lower than that presently employed. This could allow a reduction in the thickener concentration, and consequently a reduction in the cost of the retardant composition. It is therefore recommended that studies be conducted toward the determination of the effect of gum thickener concentration (and type) on the aerial dissemination characteristics of a liquid retardant.

The models developed on the program have enabled the estimation of the terminal sizes of the droplets produced by the aerial dissemination of various retardants, as well as provided further understanding of a variety of factors relating to dissemination, droplet settling and ground contour pattern. In order to make further progress and check the analyses and predictions - especially regarding terminal droplet size - it is desirable that full scale aerial dissemination tests be conducted that provide the necessary data, and such tests are recommended. The general nature of these tests was discussed previously.[1]

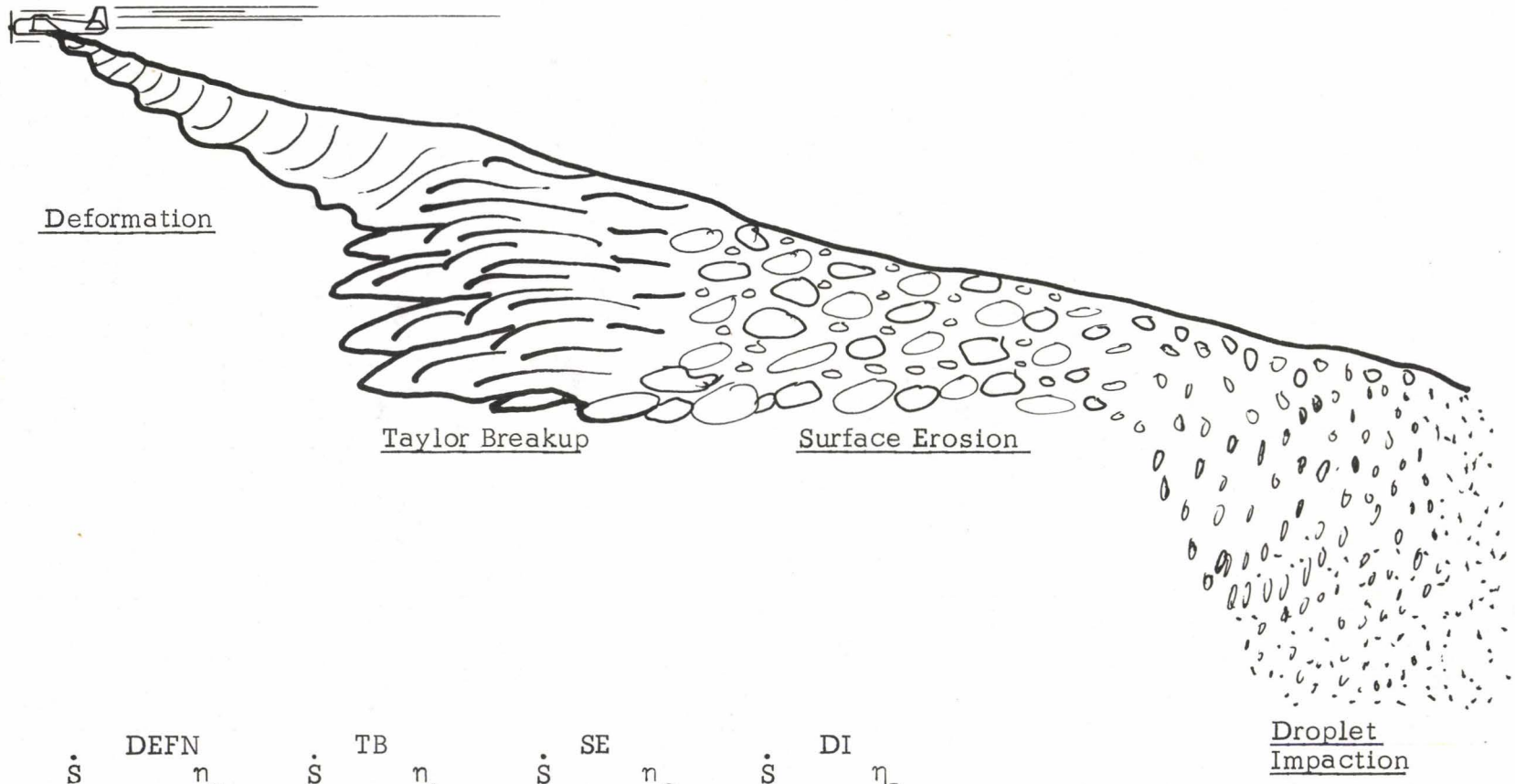

	DEFN		TB		SE		DI	
	$\dot{S}$	η_e	$\dot{S}$	η_e	$\dot{S}$	η_e	$\dot{S}$	η_a
	(sec^{-1})	poise						
PC	2.2	65	13	35	550	12	10-100	4
FT 100	2.2	101	40	6	380	0.8	10-100	4
FT 931	2.2	15	110	1.2	410	0.8	10-100	1.2
H_2O	2.4	0.01	1520	0.01	740	0.01	$\sim 10^3$	0.01

Figure 22. Summary of the Shear Rate and Viscosity of the Various Liquid Fire Retardants During Aerial Dissemination.

REFERENCES

1. W. H. Andersen, R. E. Brown, K. G. Kato and N. A. Louie, "Investigation of Rheological Properties of Aerial-Delivered Fire Retardant," Report 8990-04 (Final), to Northern Forest Fire Laboratory, U. S. Forest Service, June 1974.

2. D. H. Swanson, "High Altitude Retardant Drop Mechanization Study," Final Report, Vol. I to Northern Forest Fire Laboratory, Missoula, Montana, Honeywell, April 1973.

3. E. B. Anderson, et al, "Aerial Delivery Systems Program," Final Report, ATR-74(7299)-1, to U. S. Forest Service, The Aerospace Corporation, Dec. 1973.

4. C. W. George and A. D. Blakely, "An Evaluation of the Drop Characteristics and Ground Distribution Patterns of Forest Fire Retardants," USDA Forest Service Res. Paper INT-134, IFR Experiment Station, Ogden, Utah, March 1973.

5. C. W. George, "Effect of Drop Height on Retardant Ground Distribution Patterns from the CL-215," U. S. Forest Service Report, Missoula, Montana, Jan. 1973.

6. C. W. George and A. D. Blakely, "A Study of the Effects of Tank and Gating Characteristics on Retardant Ground Distribution Patterns," Study 2107-17C, Northern Forest Fire Laboratory, Missoula, May 1973.

7. D. H. Swanson and T. N. Helvig, "Extended High Altitude Retardant Drop Mechanization Study, January 1974.

8. O. G. Engel, J. Res. NBS 54, 281(1955).

9. F. J. Heymann, J. App. Phys. 40, 5113(1969).

10. Y. C. Huang, F. G. Hammitt and W. Yang, "Impact of Spherical Water Drop on Flat Rigid Surface," Report 933710-10-T, Univ. of Michigan, August 1971.

APPENDIX I

VELOCITY AND DISPLACEMENT OF FALLING DROPS

The velocity, v, at time, t, of a liquid droplet with mass, m, falling under the influence of gravity and retarded by air drag is determined by the differential equation

$$mg - C_d\, 0.5\, \rho\, v^2 A = m(dv/dt) \tag{1}$$

where g is the gravitational constant, C_d is the drag coefficient, ρ is air density, and A is the projected frontal cross-sectional area of the drop. Integrating Eq. (1) under conditions that $v = v_o$ at $t = 0$ gives

$$v = \frac{(g/K)^{1/2}\,[\,k \exp(Bt) - 1\,]}{[\,k \exp(Bt) + 1\,]} \tag{2}$$

$$K = 3\rho C_d / 4 \rho_1 d \tag{3a}$$

$$B = 2(Kg)^{1/2} \tag{3b}$$

$$k = \frac{g + v_o (Kg)^{1/2}}{g - V_o (Kg)^{1/2}} \tag{3c}$$

where ρ_1 is liquid density and d is droplet diameter. Equation 2 gives the falling droplet velocity as a function of time. For very large t, i.e., $t = \infty$

$$v = v_t = (g/K)^{1/2} = \left[\frac{4 \rho_1 g d}{3 \rho C_d}\right]^{1/2} \tag{4}$$

where v_t is the final terminal settling velocity of the droplet.

Integrating Eq. (1) under the initial conditions that $v = 0$ when $t = 0$ gives

$$v = \frac{(g/K)^{1/2}\,[\exp(Bt) - 1\,]}{[\,\exp(Bt) + 1\,]} \tag{5}$$

For $t = \infty$, this equation reduces to Eq. (4). This equation also follows from Eq. (2) by the substitution of $v_o = 0$.

Equation (5) gives the droplet velocity as a function of time for a falling droplet with an initial velocity of zero. The distance, y, through which the drop falls in a time t may be obtained by substituting $v = dy/dt$ in Eq. (5) and integrating under the condition that $y = 0$ when $t = 0$. The resulting equation relating fall distance to time is

$$y = (1/2K)\ \ell n \left[0.25(1 + \exp(-Bt))\,(1 + \exp(Bt))\right] \qquad (6)$$

APPENDIX II

LIQUID SPREADING CONTROLLED BY SURFACE TENSION

Consider a spherical liquid drop with density ρ_1, radius r and surface tension γ dropped from a height, H, onto a flat, non-absorbent surface. The initial potential energy of the drop before its release and subsequent impact and spreading is $V_{oi} = \rho_1 g H V$, where g is the gravitational constant and V is the drop volume ($V = (4\pi/3)r^3$). The corresponding surface energy of the drop is $V_s = 4\pi r^2 \gamma$. The drop is now released and allowed to spread radially and symmetrically over the surface of the solid until an equilibrium state is attained. It is assumed that this final state of the liquid is approximately disc shaped and has a spread area, A, (in contact with the solid surface) that is related to drop volume by

$$hA = V \tag{1}$$

where h is the average film thickness of the spread liquid on the surface. It is assumed that A is controlled by surface tension forces. The outer edge of the spread liquid makes an angle θ (the contact angle) with the solid surface. The potential energy of the spread liquid is $V_{oe} = \rho_1 ghV/2$, and its surface energy is given by $V_{se} = (\gamma + \gamma_i) A + 2\pi ah\gamma$, where γ_i is the interfacial tension of the solid in contact with the liquid, and a is the radius of the spread liquid.

An energy balance of the liquid before and after spreading gives

$$V_{oi} + V_s + \gamma_S A = V_{oe} + V_{se} \tag{2}$$

where γ_S is the interfacial tension of the solid in contact with air. From thermodynamics, $\gamma_S = \gamma_i + \gamma \cos\theta$. Substituting in Eq. (2) gives

$$(1-\cos\theta) = Bh + (24^{1/2}/d^{3/2})h^{3/2} - (\rho_1 g/2\gamma)h^2 \tag{3}$$

$$B = \frac{\rho_1 gH}{\gamma} + \frac{6}{d} \tag{4a}$$

$$h = V/A \tag{4b}$$

where d is the diameter of the (initially) spherical drop. Note that h, the film thickness, is the reciprocal of the spread factor, A/V (liquid film area per unit drop volume), which can be measured experimentally. For the static spreading of a drop, i.e., when the drop is merely placed on the surface and allowed to spread, $H = d/2$.

APPENDIX III

APPROXIMATE MODEL FOR DROP SPREAD BASED ON ENERGY CONSERVATION CONCEPTS

The following approximate model was developed which correctly describes the observed rate of spreading of a liquid drop impacting with a solid surface. In this model the drop spread is constrained only by the conservation of mass and energy.

The drop is represented at impact by a cylinder (axis normal to the plane of impact) whose initial radius, R_o, is set equal to the radius of the real drop just before impact. The height, h, of the cylinder at any time is given by

$$h = V/\pi R^2 \tag{1}$$

where V is the drop volume, and at time zero the subscript zero should be appended to the preceding equation. The initial kinetic energy, E_{ok}, of the drop is given by

$$E_{ok} = 0.5 m V_i^2 = 0.5 \rho_l V V_i^2 \tag{2}$$

where m is liquid mass, ρ_l is liquid density, and V_i is the impact velocity of the drop with the surface. The surface tension energy, E_s, of the liquid at any time during spreading is given by

$$E_s = \gamma(\pi R^2 + 2\pi R h) \tag{3}$$

where γ is liquid surface tension. At zero time the subscript zero should be appended to this equation. An energy balance of the liquid during its spreading indicates that

$$E_{ok} + E_{os} = E_k + E_s + E_v \tag{4}$$

where E_v is the instantaneous viscous energy of the liquid. Integrating the radial flow field implied by the preceding assumptions over the initial cylinder gives the instantaneous kinetic energy, E_k, of the liquid, i.e.,

$$E_k = (m v^2/12)(R/R_o)^2 \tag{5}$$

where R is the radius of the cylindrically diverging flowing liquid, and v is the liquid flow velocity at R. The viscous energy is taken to be

$$E_v = (\pi \eta/2 h_o R_o^2) \int_{R_o}^{R} v R^4 \, dR \tag{6}$$

where η is the apparent viscosity of the liquid. At the moment of impact, $R = R_o$, and hence $E_v = 0$.

Rearranging the energy balance equation gives

$$v^2 = (12/m)(R_o/R)^2 \left\{ E_{ok} - \gamma [\pi(R^2-R_o^2) + 2\pi R h_o (R_o^2/R^2-1)] \right.$$

$$\left. + (\pi \eta/2 h_o R_o^2) \int_{R_o}^{R} v R^4 \, dR \right\} \qquad (7)$$

At the moment of impact, $R = R_o$, and $v^2 = (12 E_{ok}/m) = 6V_i^2$, or $v = 2.45 V_i$. Thus the initial radial velocity is several times larger than the impact velocity. This agrees with both experimental and more rigorous analytical findings.[8-10]

The value of v in Eq. (7) is given by dR/dt, where d denotes derivative. This differential equation is solved by a numerical Runge-Kutta routine. The integral in the viscosity term is evaluated by summation over time steps as

$$\Sigma v_i R_i^4 (R_i - R_{i-1}) \qquad (8)$$

☆ U.S. GOVERNMENT PRINTING OFFICE: 1974 — 677-095 / 144 REGION NO. 8